國立臺灣大學電機資訊學院電信工程學研究所

碩士論文

Graduate Institute of Communication Engineering

College of Electrical Engineering and Computer Science

National Taiwan University

Master's Thesis

OTFS 系統中降低功率峰均比的研究

Study on the PAPR Reduction for the OTFS System

陳美如

Mei-Ru Chen

指導教授：林茂昭 博士

李晃昌 博士

Advisor: Mao-Chao Lin, Ph.D.

Huang-Chang Lee, Ph.D.

中華民國 113 年 7 月

July, 2024

doi:10.6342/NTU202402900

致謝

在這裡，我想表達我最深的感謝之情，向所有在我學術旅程中支持與幫助過我的人致以衷心的謝意。

首先，我要感謝我的指導老師林茂昭老師及李晃昌老師。您們的悉心指導和無私奉獻，不僅讓我在學術上獲得了寶貴的知識，更激勵我不斷探索與進步。您的耐心解答和建設性意見對我而言如同燈塔，指引著我前行。不只在學習方面，也感謝碩班生活中老師時常的關心．

我也想感謝實驗室的同學們：靖昌、琬甯、梵勳。與你們的合作和交流，使得碩班生活充滿了趣味。每一次討論和互助，都是我成長的一部分。你們的友善與聰慧讓這段時光變得更加充實和愉快。

同時，我的男友駿杰在這段旅程中給予了我無盡的支持和陪伴。每當我面臨困難與挑戰時，是你的鼓勵和理解讓我重拾信心，堅持不懈。你的支持成為我前行的力量與勇氣。

我要感謝我的家人。你們的支持，是我無法言喻的精神支柱。每一次的鼓勵和關懷，讓我在追尋夢想的路上倍感溫暖。你們的包容與愛護讓我在困難時不孤單，始終感受到家庭的力量。

最後，感謝我自己在這段整個求學過程中的堅持。每一步的努力和每一次的突破，都來自對目標的堅持和對未來的憧憬。希望未來能永遠記住現在自己的模樣，眼神閃閃發光．

感謝所有陪伴和支持過我的人，正是你們的幫助與鼓勵，使我能夠一路走來，完成這一階段的學習與成長。

doi:10.6342/NTU202402900

中文摘要

正交時頻空間(Orthogonal Time Frequency Space, OTFS)系統對於高速移動無線通信至關重要，能在挑戰性的環境中提供穩健的性能。然而，OTFS 系統的一個顯著問題是高峰均功率比(Peak-to-Average Power Ratio, PAPR)，這可能導致功率放大器中的非線性失真，並降低整體系統性能。傳統峰均功率比的降低方法，如μ-law 壓縮，雖然有效，但往往會導致位元錯誤率(Bit Error Rate, BER)增加，因此在降低峰均功率比和保持信號品質之間需要做權衡。

本研究探討了窗口技術在 OTFS 系統中解決高峰均功率比問題的應用。我們探索了三種類型的窗口：多普勒偏移窗口、時間延遲窗口和複合窗口。使用了包括網格搜索和參數推導在內的各種參數選擇方法來評估這些窗口技術的有效性。實驗結果表明，窗口技術顯著降低了峰均功率比，同時保持了可控的位元錯誤率增加。

儘管結果令人鼓舞，我們的研究卻有參數計算複雜度等限制。未來的研究應集中於通過先進的算法來優化窗口參數。此外，將窗口技術與其他峰均功率比減少策略結合，可能會帶來更好的性能改進。

總之，本文提供了一種在 OTFS 系統中降低峰均功率比的新方法，驗證了窗口技術的有效性，並突出了它們在不顯著增加位元錯誤率的情況下提高高速移動無線通信性能的潛力。

關鍵詞：正交時頻空間系統、峰均功率比、位元錯誤率、μ-law 壓縮、窗口技術

doi:10.6342/NTU202402900

Abstract

Orthogonal Time Frequency Space (OTFS) systems are essential for high-mobility wireless communications, providing robust performance in challenging environments. However, a significant issue in OTFS systems is the high Peak-to-Average Power Ratio (PAPR), which can cause non-linear distortions in power amplifiers and degrade overall system performance. Traditional PAPR reduction methods, such as μ-law companding, while effective, often result in increased Bit Error Rate (BER), presenting a trade-off between reducing PAPR and maintaining signal quality.

This research investigates the application of windowing techniques to address the PAPR problem in OTFS systems. We explored three types of windows: Doppler shift window, time delay window, and complex window. Various parameter selection methods, including grid search and parameters derivation, were employed to evaluate the effectiveness of these windowing techniques. Our experimental results demonstrate that windowing methods significantly reduce PAPR while maintaining a manageable increase in BER.

Despite the promising results, our study acknowledges limitations such as the computational complexity of parameter optimization. Future research should focus on optimizing window parameters through advanced algorithms. Additionally, combining

doi:10.6342/NTU202402900

windowing methods with other PAPR reduction strategies could yield even better performance improvements.

In conclusion, this thesis provides a novel approach to PAPR reduction in OTFS systems, validating the effectiveness of windowing techniques and highlighting their potential for enhancing high-mobility wireless communications without significantly increasing BER.

Keywords: Orthogonal Time Frequency Space (OTFS) systems, Peak-to-Average Power Ratio (PAPR), Bit Error Rate (BER), μ-law companding, Windowing techniques

doi:10.6342/NTU202402900

Contents

doi:10.6342/NTU202402900

doi:10.6342/NTU202402900

doi:10.6342/NTU202402900

List of figures

doi:10.6342/NTU202402900

doi:10.6342/NTU202402900

List of tables

doi:10.6342/NTU202402900

Chapter 1 Introduction

1.1 Motivation

In modern wireless communication systems, achieving high data rates with robust performance is essential. Orthogonal Time Frequency Space (OTFS) modulation has emerged as a promising technique to address the challenges posed by high-mobility environments, such as those encountered in vehicular and high-speed train communications.[1] OTFS offers enhanced performance in handling the Doppler and delay spreads typically experienced in such scenarios.[2] Despite its advantages, OTFS systems face a significant challenge: the high Peak-to-Average Power Ratio (PAPR) of the transmitted signal.[3] High PAPR can lead to power inefficiencies and distortions in power amplifiers, which degrade the overall system performance.[4]

Traditional methods for reducing PAPR, such as μ-law companding, have been employed with some success.[5] However, these methods often result in a considerable increase in the Bit Error Rate (BER), which limits their practical effectiveness. The high BER can counteract the benefits of PAPR reduction, making it imperative to find alternative solutions that can balance both requirements effectively.

1.2 Contribution

Our research addresses this challenge by exploring the use of windowing techniques

doi:10.6342/NTU202402900

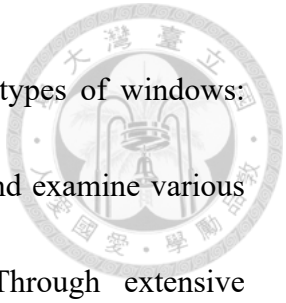

to reduce PAPR in OTFS systems. We investigate three different types of windows: Doppler shift window, time delay window, and complex window, and examine various parameter selection methods to optimize their performance. Through extensive experimentation, we demonstrate that windowing techniques can achieve significant PAPR reduction while maintaining a manageable BER. This finding suggests that windowing techniques can be a viable and effective alternative to traditional PAPR reduction methods.

The primary contributions of this research are as follows:

1. We propose and design three novel windowing techniques specifically tailored for PAPR reduction in OTFS systems.
2. We develop and evaluate different parameter selection methods, including derivation for Doppler shift window and grid search, to optimize the windowing techniques.
3. We provide a comprehensive analysis of the trade-offs between PAPR reduction and BER performance, highlighting the advantages of windowing techniques over traditional methods.
4. We validate our proposed methods through numerical simulations, demonstrating their effectiveness in reducing PAPR without significantly increasing BER.

doi:10.6342/NTU202402900

1.3 Structure of the thesis

The structure of this thesis is organized as follows:

Chapter 1 provides an introduction to the motivation, problem definition, primary contributions, and the overall structure of the thesis.

Chapter 2 offers an in-depth introduction to OTFS, covering the system model, channel response representation, MMSE equalization, PAPR characteristics of OTFS signals, and the use of μ-law companding to reduce PAPR.

Chapter 3 delves into the proposed windowing techniques for PAPR reduction, detailing the design of Doppler shift, time delay, and complex windows. It also discusses the selection methods for window parameters, including derivation and grid search approaches.

Chapter 4 presents the numerical results, focusing on the effectiveness of the proposed windowing techniques in reducing PAPR and their impact on BER.

Chapter 5 concludes the thesis, summarizing the findings and suggesting future research directions, such as the optimization of window parameters and the combination of windowing techniques with other existing PAPR reduction methods.

This research aims to provide a comprehensive solution to the PAPR problem in OTFS systems, enhancing their performance and paving the way for more efficient and reliable

doi:10.6342/NTU202402900

high-mobility communications.

doi:10.6342/NTU202402900

Chapter 2 Background Knowledge

2.1 OTFS system framework

A typical system model of OTFS is shown in Figure 2.1.

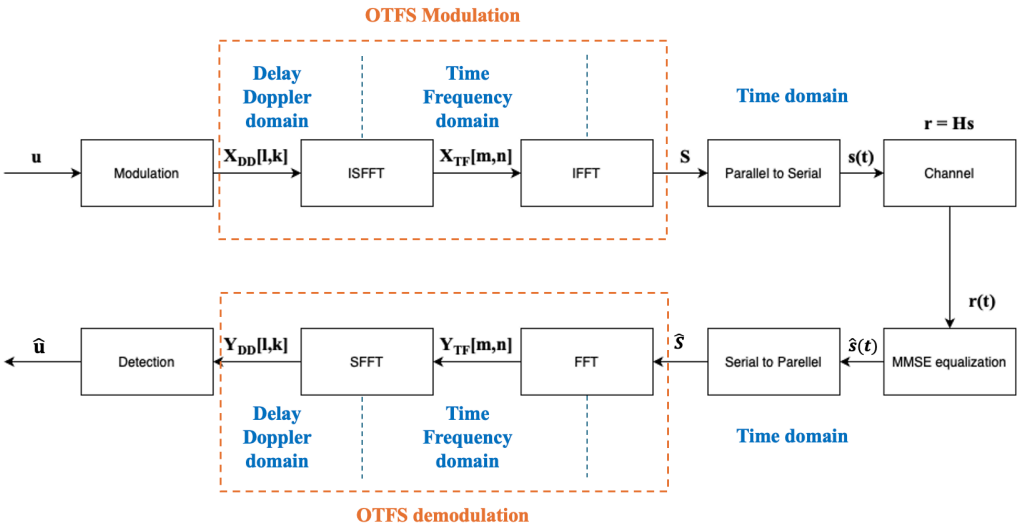

Figure 2.1 OTFS system framework

2.2 OTFS system transmitter

In a single OTFS frame containing M delays and N dopplers, there are $M \times N$ information samples $X_{DD}[l,k]$ in the delay-Doppler (DD) domain, with l and k represent indices for the delay and Doppler dimensions, respectively.[6]

Each information symbol can be allocated a specific modulation scheme, such as quadrature amplitude modulation (QAM) or phase shift keying (PSK).

The DD domain signals $X_{DD}[l,k]$ are modulated using a 2D inverse symplectic finite

doi:10.6342/NTU202402900

Fourier transform (ISFFT). It converts the DD domain signals into the time-frequency domain signal $X_{TF}[m,n]$, where m is the subcarrier index, and n is the time slot index.

The output of ISFFT can be written as:

$$X_{TF}[m,n] = \frac{1}{\sqrt{NM}} \sum_{k=0}^{N-1} \sum_{l=0}^{M-1} X_{DD}[l,k] e^{j2\pi\left(\frac{nk}{N} - \frac{ml}{M}\right)} \quad (2.1)$$

$$= \frac{1}{\sqrt{NM}} \sum_{l=0}^{M-1} e^{j2\pi\left(-\frac{ml}{M}\right)} \sum_{k=0}^{N-1} X_{DD}[l,k] \, e^{j2\pi\left(\frac{nk}{N}\right)} \quad (2.2)$$

It could also be written in matrix form:

$$X_{TF} = F_M X_{DD} F_N^H \quad (2.3)$$

where F_M denotes $M \times M$ normalized discrete Fourier transform (DFT) matrix, and F_N^H denotes $N \times N$ normalized inverse discrete Fourier transform (IDFT).

Then Discrete Heisenberg Transform transfers the time-frequency domain signal $X_{TF}[m,n]$ to the transmit signal in the time delay domain (time domain) using an M-point IDFT:

$$s(t) = \sum_{n=0}^{N-1} \sum_{m=0}^{M-1} X_{TF}[m,n] e^{j2\pi m\Delta f(t-nT)} \quad (2.4)$$

The process of the above equations (2.1) to (2.4) can be represented by the Figure 2.2.

doi:10.6342/NTU202402900

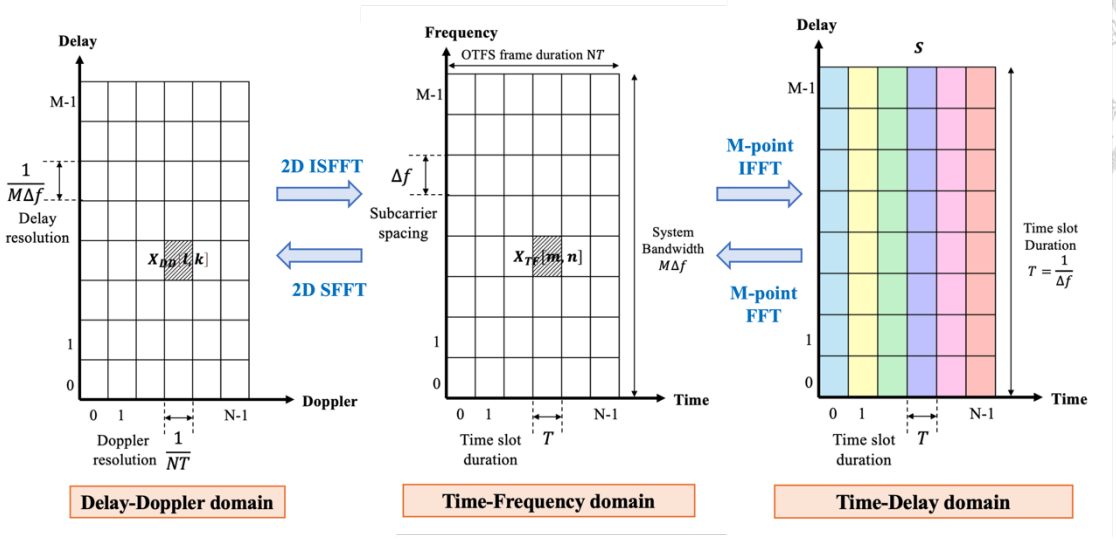

Figure 2.2 Conversion of OTFS signal (from DD to TF to time)

The time domain transmit signal matrix is given by [1]：

$$S_{M\times N} = F_M^H X_{TF} = F_M^H (F_M X_{DD} F_N^H) = X_{DD} F_N^H \quad (2.5)$$

The process of the above equation (2.5) can be represented by the Figure 2.3.

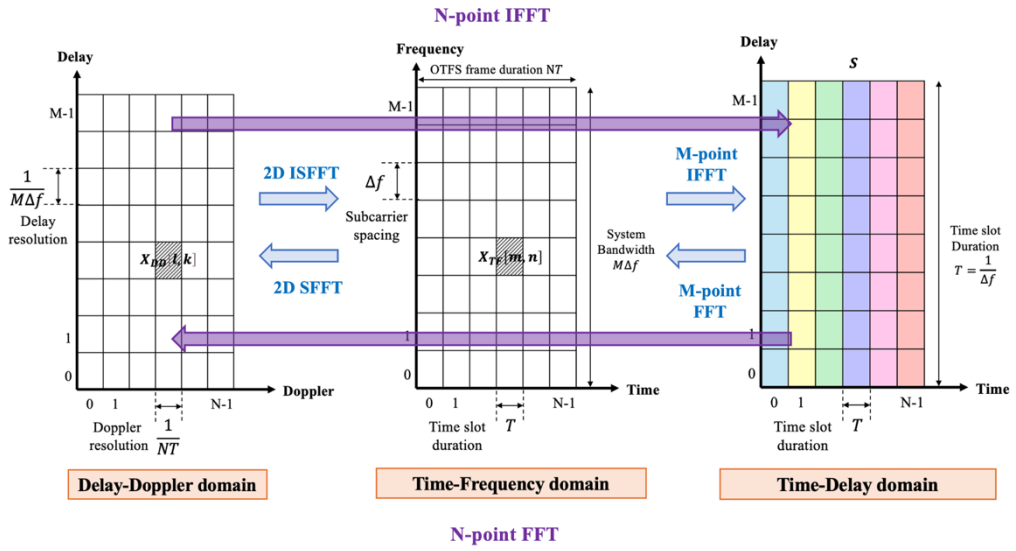

Figure 2.3 Conversion of OTFS signal (from DD to time)

doi:10.6342/NTU202402900

The corresponding time domain transmit signal represented as a row vector s is obtained by

$$s_{1\times MN} = vec(S_{M\times N}) = (F_N^H \otimes I_M)vec(X_{DD}) = (F_N^H \otimes I_M)x \quad (2.6)$$

where $\otimes$ is the Kronecker product of two matrices.

We can use Figure 2.4 to represent this process more intuitively.

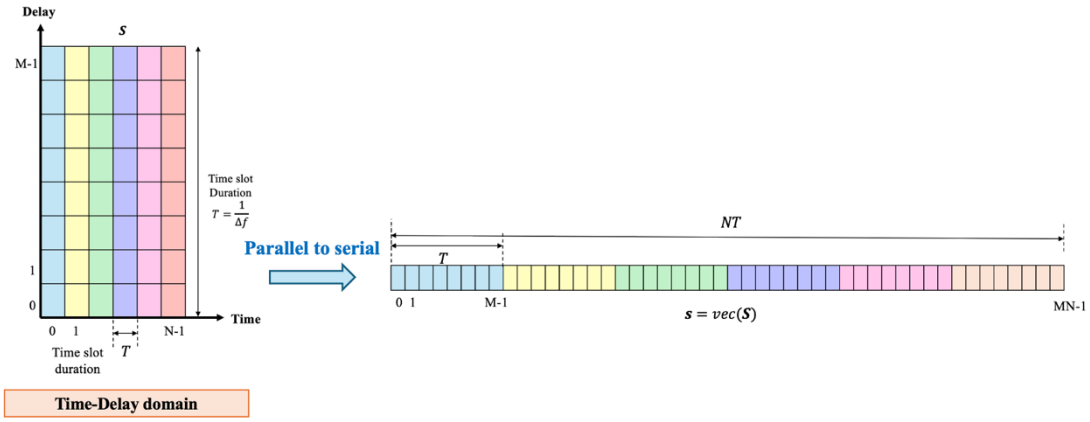

Figure 2.4 Transform parallel time signal to serial

2.3 Cyclic prefix of OTFS signal

In Orthogonal Time Frequency Space (OTFS) systems, the Cyclic Prefix (CP) plays a crucial role in maintaining the integrity and performance of the transmitted signal. The CP is a technique used to combat inter-symbol interference (ISI) caused by multipath propagation in wireless communication channels. By adding a CP, OTFS systems can efficiently handle the channel's delay spread and enhance the system's robustness against time dispersion effects.

doi:10.6342/NTU202402900

There are two types of CP in OTFS: full CP and reduced CP.[7]

2.3.1 Full cyclic prefix

Full CP involves appending a CP to each symbol that is equal in length to the maximum expected delay spread of the channel. This is achieved by copying the last part of the signal and pasting it at the beginning of the frame of OTFS signal in Delay-Doppler domain.[8] It provides the most robust protection against ISI and maintains the orthogonality of the entire symbol duration. However, the primary drawback is the overhead. A full CP significantly reduces the spectral efficiency as a considerable portion of the transmitted data is redundant.

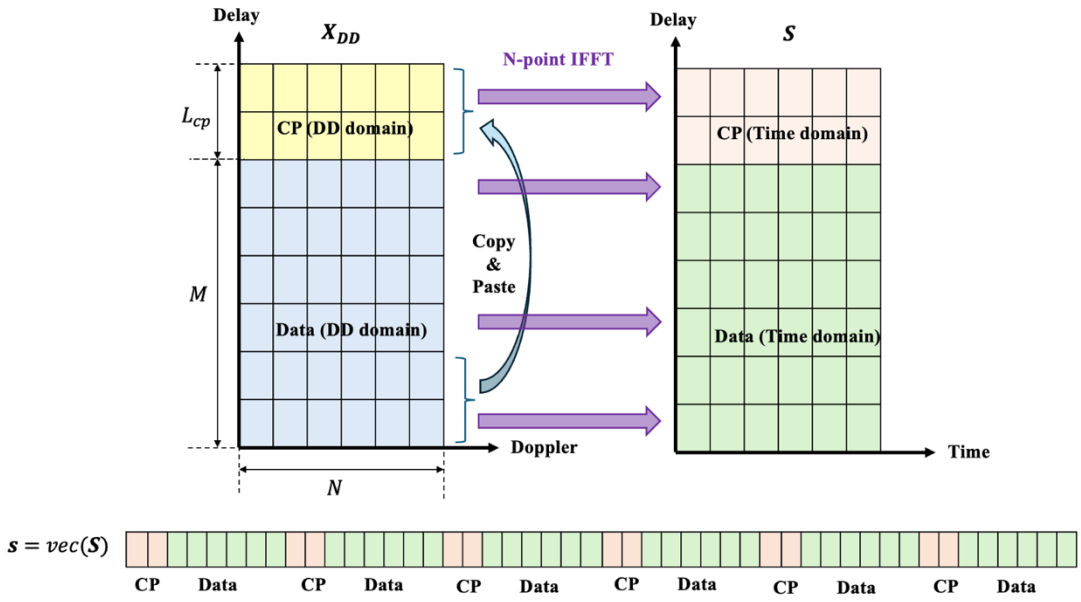

Figure 2.5 full cyclic prefix

doi:10.6342/NTU202402900

2.3.2 Reduced cyclic prefix

Reduced CP is shorter than the maximum delay spread of the channel. It is a compromise between the robustness of full CP and the need to improve spectral efficiency. This is done by copying a shorter segment from the end of the whole signal and pasting it at the beginning in the time domain.[7] It reduces the overhead associated with the CP, thereby increasing the spectral efficiency and allowing more data to be transmitted. While it offers improved efficiency, reduced CP may not fully mitigate ISI, potentially leading to a slight degradation in performance, especially in highly dispersive channels.

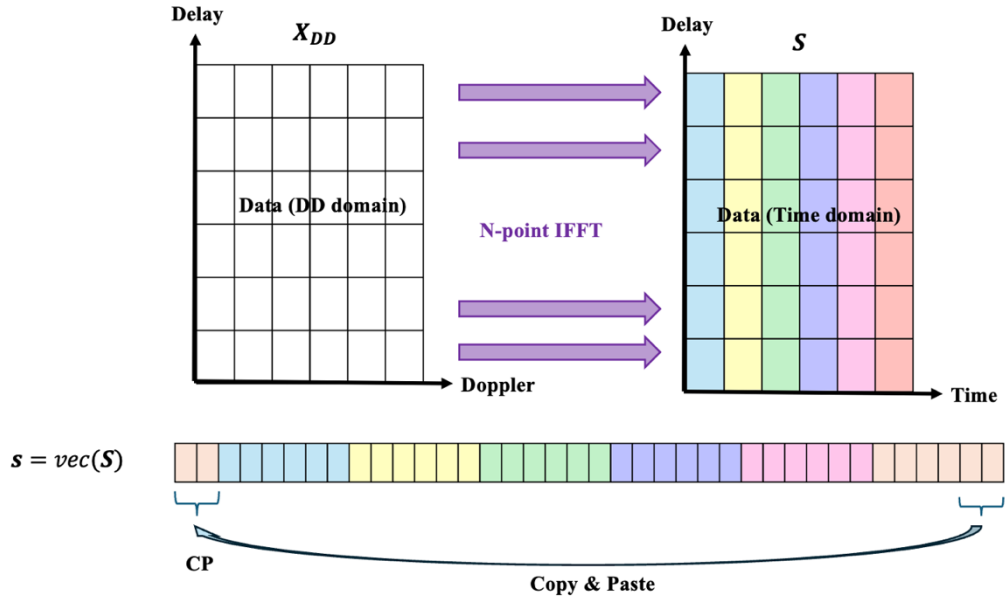

Figure 2.6 reduced cyclic prefix

2.4 Channel Response

Typically, the channel has only a few reflectors, each with associated delays and

doi:10.6342/NTU202402900

Doppler shifts. As a result, only a limited number of parameters are necessary to model the channel in the Delay-Doppler domain. Due to this sparsity, it is convenient to represent the time-varying channel response in Delay-Doppler domain as:[9]

$$h_{DD}(\tau,\nu) = \sum_{i=1}^{L} h_i \delta(\tau - \tau_i)\delta(\nu - \nu_i) \quad (2.7)$$

where L is the number of resolvable paths, $h_i \in C$ is the channel coefficient of the i-th path, $\tau_i \in [0, \tau_{max}]$ denote the delay of the i-th path, and $\nu_i \in [0, \nu_{max}]$ denote the Doppler shifts of the i-th path.

The delay and Doppler-shift taps for i-th path are given by

$$\tau_i = \frac{l_i}{M\Delta f}, \nu_i = \frac{k_i}{NT} \quad (2.8)$$

where $M\Delta f$ and NT denote the total bandwidth and duration of the transmitted signal frame, respectively. To simplify the derivations, we assume l_i and k_i are integers. Moreover, $l_i < M$ and $k_i < N$.

Consequently, the received signal can be expressed as:

$$r(t) = \int_{-\infty}^{\infty}\int_{-\infty}^{\infty} h_{DD}(\tau,\nu) e^{j2\pi\upsilon(t-\tau)} s(t-\tau) d\tau d\upsilon + z(t) \quad (2.9)$$

Where $z(t)$ is the additive white Gaussian noise (AWGN) in the time domain.

As referenced in [9], the channel response can also be represented in matrix form:

$$\mathrm{H} = \sum_{i=1}^{L} h_i \Pi^{l_i} \Delta^{k_i} \quad (2.10)$$

doi:10.6342/NTU202402900

where H is a $MN \times MN$ time domain channel matrix with L paths, Π is the permutation matrix, and Δ is the diagonal matrix

$$\Pi = \begin{bmatrix} 0 & \dots & 0 & 1 \\ 1 & \ddots & \ddots & 0 \\ \vdots & \ddots & \ddots & \vdots \\ 0 & \dots & 1 & 0 \end{bmatrix}_{MN \times MN} \quad (2.11)$$

$$\Delta = \begin{bmatrix} 1 & \dots & 0 & 0 \\ 0 & e^{\frac{j2\pi}{MN}} & \ddots & 0 \\ \vdots & \ddots & \ddots & \vdots \\ 0 & \dots & 0 & e^{\frac{j2\pi(MN-1)}{MN}} \end{bmatrix}_{MN \times MN} \quad (2.12)$$

Here, the matrices Π and Δ correspond to the delays and Doppler shifts in equation (2.10), respectively. Each path causes a l_i-step cyclic shift in the transmitted signal vector s, represented by Π^{l_i}, and modulates it with a carrier frequency k_i, represented by Δ^{k_i}. Hence, we can rewrite equation (2.9) in vector form as:

$$r = \mathrm{H}s + w \quad (2.13)$$

where w is the additive white Gaussian noise (AWGN) vector with mean 0 and covariance matrix $\gamma^{-1} I_{MN}$.

2.5 Equalizer

In the OTFS system, equalization techniques are employed to counteract the effects of channel impairments and recover the original transmitted signals. Based on the characteristics of equalization techniques, they can be classified into two categories:

doi:10.6342/NTU202402900

linear and non-linear.

Among them, Non-linear equalizers achieve performance close to maximum likelihood (ML) but come with an iterative structure and high complexity. One of common non-linear equalizer is the Message Passing (MP) based detector proposed by [10] and [11]. To reduced the complexity of MP algorithm,[12] proposed the Approximate Message Passing (AMP) algorithm based on covariance processing. [13] used Markov Chain Monte Carlo (MCMC) method in detection of OTFS.

In contrast, linear equalizers have a simpler structure, though their performance is inferior to that of non-linear equalizer. Conventional linear equalizers include linear minimum mean square error (MMSE) receiver which has a log-linear order of complexity [14] and zero-forcing (ZF) equalizers referring to [15].

In this thesis, we use the low complexity linear minimum mean square error (MMSE) equalizer in signal detection of OTFS system, which can mitigate both Inter-Carrier Interference (ICI) and Inter-Symbol Interference (ISI) effectively in communication systems.

As mentioned in [15], the linear transformation matrices for MMSE is given by:

$$\hat{s} = \mathrm{H}^{\mathrm{H}}(\mathrm{H}\mathrm{H}^{\mathrm{H}} + \gamma^{-1}\mathrm{I}_{\mathrm{MN}})^{-1}r \qquad (2.14)$$

Where $\gamma = \frac{E_S}{N_0}$ is the signal-to-noise ratio (SNR). Observe that the computation of

doi:10.6342/NTU202402900

equation (2.14) involves inversion of $MN \times MN$ matrices, which has a computational complexity of $O(M^3N^3)$. This is not attractive for large values of M and N, so the equalizers have to choose carefully.

2.6 OTFS receiver

At the receiver, we reverse the transmitter operations to convert the received signal samples $\hat{s}$ into the time domain symbols $\hat{\mathrm{S}}$:

$$\hat{S} = vec^{-1}(\hat{s}) \tag{2.15}$$

This process involves folding the $1 \times MN$ row vector elements back into a rectangular $M \times N$ matrix.

Next, we can transform the received time domain signal $\hat{S}$ to the time-frequency domain signal $Y_{TF}[m,n]$ by M-point discrete Fourier transform (DFT). The time-frequency domain signal matrix can be written as:[16]

$$Y_{TF} = F_M \hat{S} \tag{2.16}$$

Then, we convert time-frequency domain symbols Y_{TF} to Delay-Doppler domain by applying symplectic finite Fourier transform (SFFT). The output of SFFT can be express as:

$$Y_{DD} = F_M^H Y_{TF} F_N \tag{2.17}$$

doi:10.6342/NTU202402900

At the same time, we can observe that by substituting equation (2.16) into equation (2.17), we can transform the time-frequency domain symbols Y_{TF} to Delay-Doppler domain just by a N-point discrete Fourier transform (DFT). It is more quickly and in lower complexity:

$$Y_{DD} = F_M^H Y_{TF} F_N = F_M^H F_M \hat{S} F_N = \hat{S} F_N \quad (2.18)$$

2.7 Definition of PAPR

Let's assume the transmitted samples of the OTFS signal are as given in equation (2.4). For one frame, the Peak to Average Power Ratio (PAPR) of the transmitted OTFS time signal $s(t)$ with symbol T_s is defined as follows:[3]

$$PAPR = \frac{\max_{0 \le t \le T_s} |s(t)|^2}{P_{av}} \quad (2.19)$$

Since $X_{DD}[l,k]$ are information symbols from a modulation alphabet, they can be treated independent and identically distributed (i.i.d.) and assumed to follow the complex Gaussian distribution with mean zero and variance $\sigma^2 = E\{X_{DD}[l,k]^2\}$.[3]

As for the average power P_{av} of transmitted signal $s(t)$ can be expressed as:

$$P_{av} = \frac{1}{T_s} \int_0^{T_s} |s(t)|^2 dt \quad (2.20)$$

Base on the Law of Large Numbers(LLN), when $MN \to +\infty$, P_{av} is given by:[17]

$$P_{av} = \frac{1}{T_s} \int_0^{T_s} |s(t)|^2 dt \quad (2.21)$$

According to the derive in [18], P_{av} in equation (2.21) can reduced as

doi:10.6342/NTU202402900

$$P_{av} = \frac{\sigma^2}{NT_s} \sum_{n=0}^{N-1} \int_0^{T_s} g_{tx}^2(t - nT) dt \quad (2.22)$$

2.8 Upper bound of PAPR

From [4], the upper bound of Peak to Average Power Ratio of transmitted OTFS signal can be bounded as:

$$PAPR \leq \frac{M^2 N^2 \max_{l,k} |X_{DD}[l,k]|^2}{M^2 N \sigma^2} \quad (2.23)$$

$$PAPR_{max} = \frac{N \max_{l,k} |X_{DD}[l,k]|^2}{\sigma^2} \quad (2.24)$$

It is noteworthy that the upper bound on the PAPR of an OTFS transmitted signal increases linearly with N and not with M. This is a distinctive characteristic of OTFS modulation, setting it apart from other multicarrier modulations, where the PAPR is dependent on the number of subcarriers (M) and increases linearly with the number of subcarriers utilized.

2.9 CCDF of PAPR

Furthermore, since PAPR is a random variable, its statistical properties can be described using the Complementary Cumulative Distribution Function (CCDF). For a given reference level $\gamma > 0$, the probability of the PAPR exceeding this reference value is determined by the CCDF, which can be described as follows:[4]

$$CCDF(\gamma) = Pr\,(PAPR > \gamma) \quad (2.25)$$

doi:10.6342/NTU202402900

where $Pr(\cdot)$ represents the probability function.

For simplicity, we consider OTFS modulation with a rectangular pulse. The time domain samples of the OTFS transmitted signal with a rectangular pulse are essentially the N-point IDFT values of the symbols in the delay-Doppler domain. Therefore, if N is large, the Central Limit Theorem suggests that the transmitted samples can be approximated as having a complex Gaussian distribution with zero mean. [9]

Therefore, as mentioned in [4], the instantaneous envelope $|s(t)|$ is Rayleigh distributed, and consequently, the instantaneous-to-average power ratio (IAPR) of each time domain sample follows an exponential distribution.

Where the definition of IPAR is:

$$IAPR = \frac{|s(t)|^2}{E\{|s(t)|^2\}} \quad (2.26)$$

and the probability that the IAPR does not exceed a threshold γ_0 is given by:

$$Pr(IAPR \leq \gamma_0) \approx (1 - e^{-\gamma_0}) \quad (2.27)$$

If we assume that the transmitted samples are mutually uncorrelated, as is the case for Nyquist sampling (with an oversampling ratio of 1), then the probability that the PAPR of the transmitted OTFS signal within a frame remains below γ_0 is expressed as:

$$Pr(PAPR \leq \gamma_0) \approx \prod_{i=0}^{NM-1}(1 - e^{-\gamma_0}) = (1 - e^{-\gamma_0})^{MN} \quad (2.28)$$

It's important to note that the assumption of uncorrelated transmitted samples doesn't hold

doi:10.6342/NTU202402900

true when the transmit signal is oversampled [4]. Therefore, the CCDF of PAPR is now expressed as follow:

$$Pr(PAPR > \gamma_0) \approx 1 - (1 - e^{-\gamma_0})^{MN} \quad (2.29)$$

Note that in OTFS, the PAPR is limited by $PAPR_{max}$ as derived in the section 2.8, meaning $Pr(PAPR > \gamma_0) = 0$ for $\gamma_0 > PAPR_{max}$.

However, equation (2.29) does not fully capture this constraint. Therefore, (2.29) serves as an approximation to the true CCDF. The actual CCDF of PAPR approaches the CCDF in (2.29) as $N \to \infty$.

2.10 Motivation of PAPR reduction

Despite its advantages in combating channel fading and improving performance in time-varying environments, OTFS modulation also tends to cause high peak-to-average power ratio (PAPR). This character arises from the transformation of symbols from the delay-Doppler domain to the time-frequency domain, which can cause large instantaneous power fluctuations.

Reducing the Peak-to-Average Power Ratio (PAPR) in OTFS modulation is critical for several reasons. High PAPR forces power amplifiers to operate in a less efficient region, requiring a significant back-off from their maximum output power, which increases energy consumption and operational costs.[19]

doi:10.6342/NTU202402900

To achieve maximum transmit power, the input signal power must be maintained within the HPA's linear region to avoid reaching the saturation point, as HPAs have a limited linear range. However, signals with high peak power can drive the HPA into saturation, resulting in in-band distortion and out-of-band power emissions. Additionally, the efficiency of the power amplifier is greatly influenced by the Peak-to-Average Power Ratio (PAPR). For class-A amplifiers, the relationship between power amplifier efficiency and PAPR is described in [20] as follows:

$$\eta = \frac{0.5}{PAPR} \times 100\% \quad (2.30)$$

where η denotes the power amplifier efficiency. Thus, the higher the PAPR, the lower the efficiency of a power amplifier. Therefore, the most effective way to maximize the efficiency of a power amplifier is to reduce PAPR. In practice, the transmitted signals are backed off before being applied to the HPA to prevent the instantaneous high peak power values from causing saturation.[20]

Otherwise, this inefficiency is particularly problematic in battery-powered devices, where it leads to faster battery depletion and reduced device lifespan. Such distortions also result in spectral regrowth, leading to interference with adjacent channels and reducing spectral efficiency. Lowering the PAPR is thus essential for maintaining signal integrity, complying with spectral regulations, and ensuring higher data rates and system

doi:10.6342/NTU202402900

capacity through the reliable use of higher-order modulation schemes. By addressing these issues, reducing PAPR enhances the overall efficiency, reliability, and cost-effectiveness of communication systems using OTFS modulation.[18, 19]

2.11 Traditional PAPR reduction techniques

Reducing the Peak-to-Average Power Ratio (PAPR) in Orthogonal Time Frequency Space (OTFS) systems is crucial for enhancing performance and efficiency. Some traditional methods used to reduce Peak-to-Average Power Ratio (PAPR) in OFDM can also be applied to OTFS, though they may require adaptation to suit the unique characteristics of OTFS. Here are several common PAPR reduction techniques used in OTFS. These methods share similarities between OFDM and OTFS, but their implementation in OTFS requires careful consideration of the differences in signal processing between the two modulation schemes.

2.11.1 Clipping and Filtering

Clipping reduces PAPR by truncating the signal's peaks, but this process can introduce both in-band and out-of-band distortion.[21] To address this, filtering is subsequently applied to mitigate the distortion. By iterative clipping and filtering, this technique can achieve a balance between reducing PAPR and maintaining signal quality.

However, the iterative nature of the iterative clipping and filtering (ICF) method

doi:10.6342/NTU202402900

requires multiple rounds of clipping and filtering, which can be computationally intensive. This increased complexity can lead to longer processing times and higher power consumption, which may not be suitable for resource-constrained devices.

2.11.2 Selective Mapping

Selective Mapping (SLM) generates multiple versions of the same OTFS symbol, each with different phase perturbations. These versions are usually produced using a predefined codebook or an optimization process. Each candidate signal represents a possible transmission option. The PAPR is calculated for each candidate signal. The candidate signal with the lowest PAPR is then selected for transmission. To ensure correct demodulation at the receiver, details about the selected candidate signal are typically transmitted along with the main signal. This side information allows the receiver to undo the phase perturbation and retrieve the original data. SLM is a powerful technique for reducing PAPR, offering a good compromise between complexity and performance. However, it does add some signaling overhead and depends on the effectiveness of the optimization process used to select the phase perturbations.[19]

2.11.3 Active Constellation Extension (ACE)

Active Constellation Extension (ACE) involves selectively extending the constellation points of a modulation scheme beyond their original positions in a controlled

doi:10.6342/NTU202402900

manner. This extension reduces the peaks in the transmitted signal, thereby lowering the PAPR. The primary goal is to find an optimal extension that minimizes PAPR without significantly affecting the error performance of the system.

Active Constellation Extension (ACE) offers a powerful method for reducing PAPR in OTFS systems, bringing benefits such as improved power efficiency and minimal impact on BER. However, these advantages come with trade-offs, including increased computational complexity and potential implementation challenges. When considering ACE for PAPR reduction in OTFS, it's essential to weigh these pros and cons to determine the best approach for the specific application and system requirements.

2.11.4 Mu-law companding

Mu-law companding is a technique used to reduce the PAPR in communication systems, including OTFS systems. High PAPR is a common issue in multicarrier modulation schemes, and companding is an effective method to address it.[3]

Mu-law companding is a logarithmic compression technique widely used in digital communication systems to enhance the dynamic range of audio signals. It can also be applied to reduce PAPR in OTFS systems. The companding process involves compressing the signal before transmission and expanding it back to its original form at the receiver.

First, applying the mu-law function to the OTFS-modulated signal before

doi:10.6342/NTU202402900

transmission, it will increase amplitude of weaker signals and decrease the amplitude of stronger signals, which will cause to alter the dynamic range of the signals. According to [3], the mu-law companding function is given by:

$$F_{\mu}(x) = sign(x)\frac{\ln(1+\mu|x|)}{\ln(1+\mu)} \quad (2.31)$$

Where x is the input signal and $sign(\cdot)$ is the sign function, which preserves the sign of x.

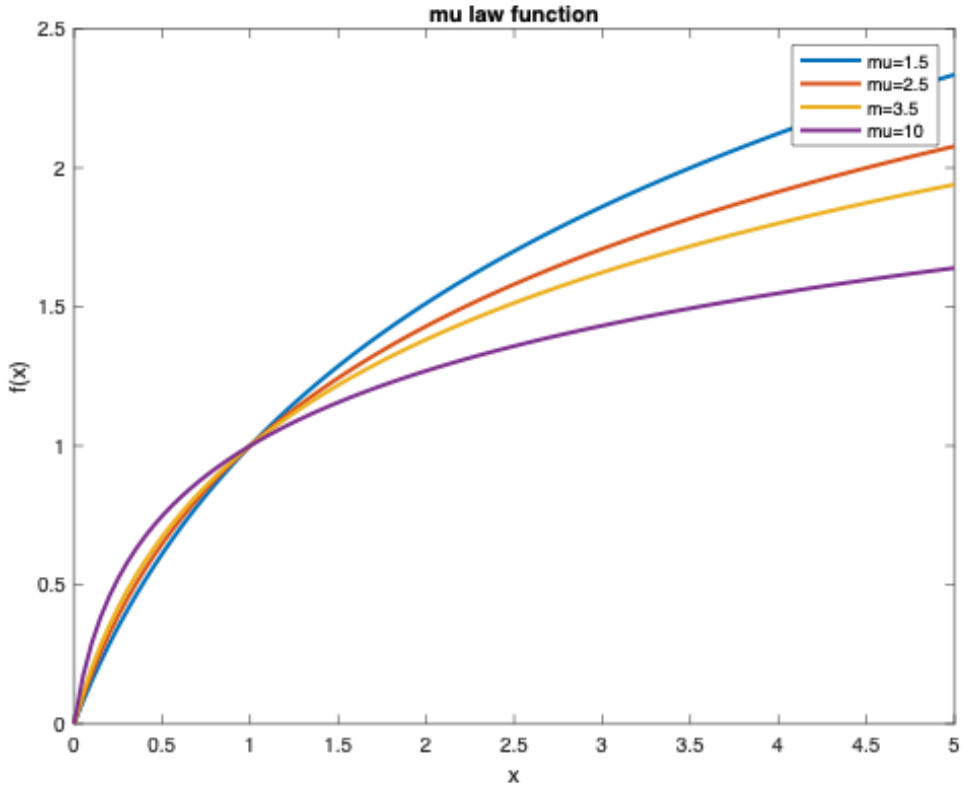

Figure 2.7 mu-law function of different mu values

Also, we should choose the non-linear compression parameter μ appropriately. Because the signal we transmitted is complex number, we can modify the equation (2.31)

doi:10.6342/NTU202402900

to:

$$s_\mu(t) = F_\mu(s(t)) = \arg(s(t)) \frac{\ln(1+\mu|s(t)|)}{\ln(1+\mu)} \quad (2.32)$$

here $\arg(\cdot)$ is the argument operation for detecting the phase of the complex signal $s(t)$.

Then, let equation (2.13) be modified as:

$$r_\mu = \mathrm{H}s_\mu + w \quad (2.33)$$

This reduces the amplitude variations of the signal, thereby lowering the PAPR, leading to more efficient power amplification and less distortion.

Second, at the Receiver, the received are recovered by:

$$\widehat{s_\mu} = \mathrm{H}^{\mathrm{H}}(\mathrm{H}\mathrm{H}^{\mathrm{H}} + \gamma^{-1}\mathrm{I}_{\mathrm{MN}})^{-1} r_\mu \quad (2.34)$$

Next, the compressed signal is expanded back to its original dynamic range using the inverse of the mu-law function.

$$F_\mu^{-1}(y) = sign(y) \frac{(1+\mu)^{|y|}-1}{\mu} \quad (2.35)$$

As the reason stated in previous, we use the equation (2.35) to deal with the complex signal:

$$\hat{s}(t) = F_\mu^{-1}\left(\widehat{s_\mu}(t)\right) = \arg(\widehat{s_\mu}(t)) \frac{(1+\mu)^{|\widehat{s_\mu}(t)|}-1}{\mu} \quad (2.36)$$

This restores the original signal with reduced distortion and noise, while preserving the benefits of reduced PAPR.

shows the block diagram of OTFS with mu-law companding technique.

doi:10.6342/NTU202402900

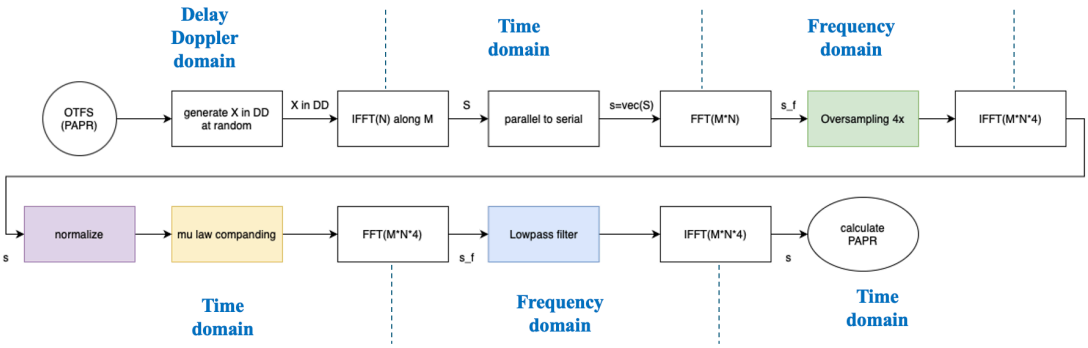

Figure 2.8 The flow diagram of mu-law companding

Meanwhile, we can note that as the μ value increases, PAPR gets decreases and BER gets increased. The following simulation result is conducted using OTFS with parameters $M = 8$ and $N = 16$, and an oversampling factor of 4. The number of blocks used in the simulation is 10^3 for PAPR and 10^5 for bit error rate (BER) respectively. The channel model is a Rayleigh fading channel with 3 paths, and the noise model is additive white Gaussian noise (AWGN). For detection, the minimum mean square error (MMSE) method is employed.

doi:10.6342/NTU202402900

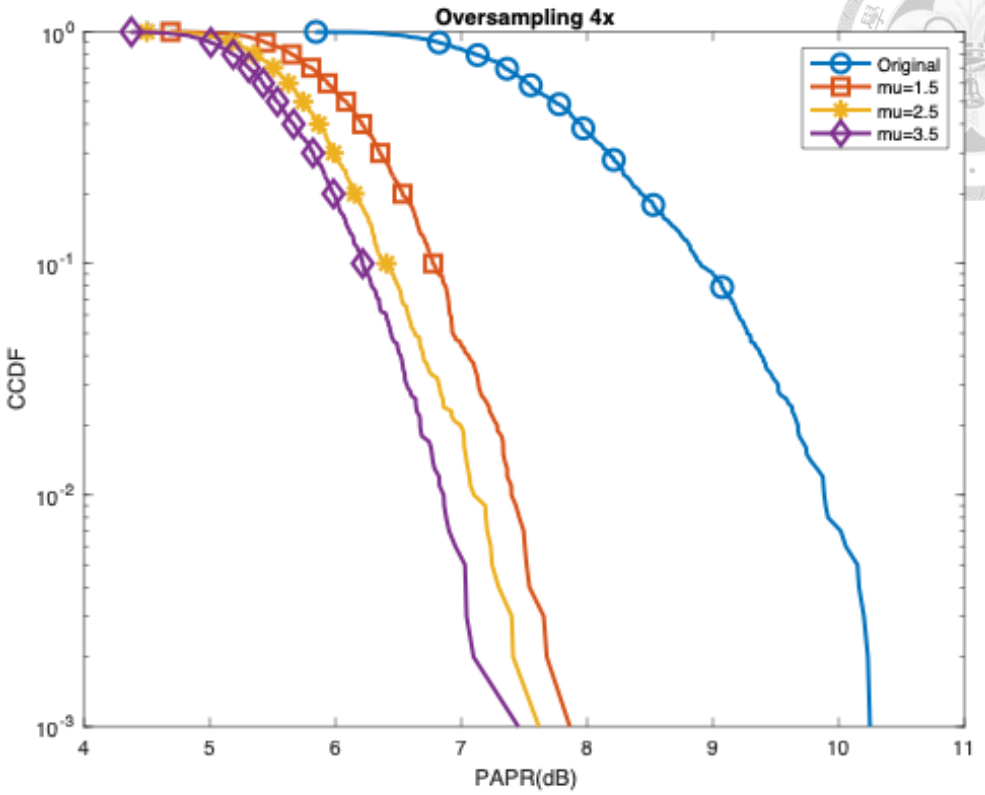

Figure 2.9 The CCDF curves of PAPR with different mu values

doi:10.6342/NTU202402900

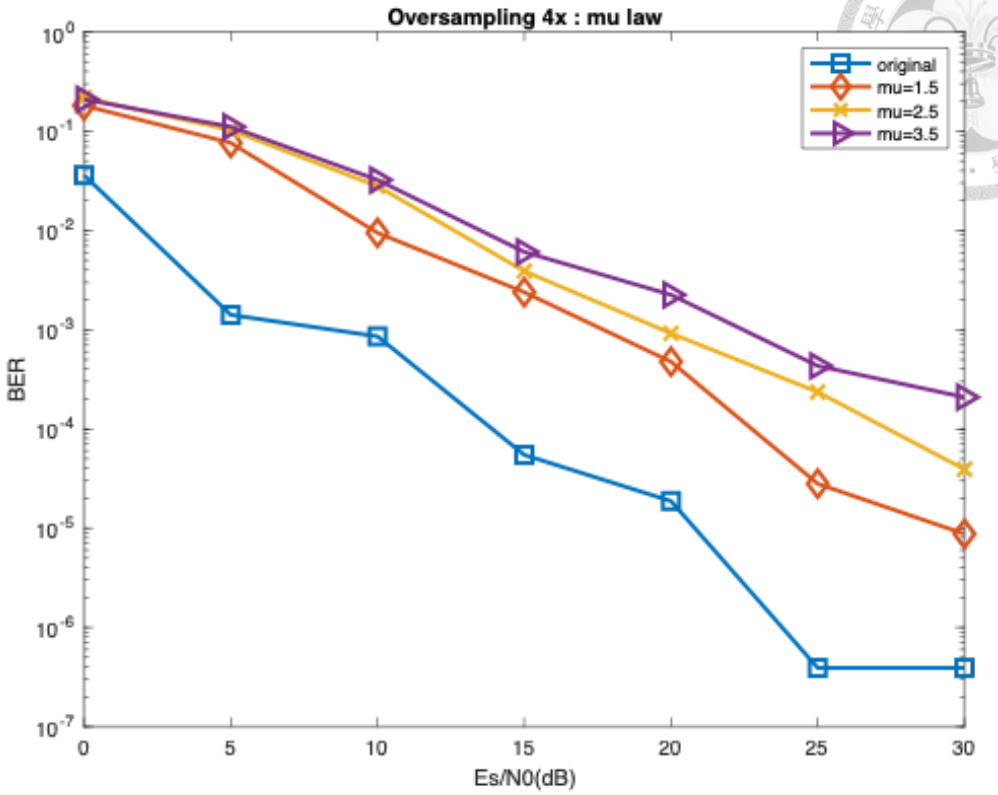

Figure 2.10 The BER curves of mu law companding with different mu values.

doi:10.6342/NTU202402900

Chapter 3 Reduce PAPR using purposed window

3.1 Windows designed for PAPR reduction Doppler shift window

Suppose that the transmitted signal $s(t)$ is multiplied to a window $G_{doppler}$ in time domain to reduce PAPR.

To represent a window function, the following mathematical expression can be used:

$$G_{doppler} = a_0 I_{MN} + a_1 \Delta^{f_1} \tag{3.1}$$

Here $a_0 = \sqrt{(1 - \|a_1\|^2)}$, and the parameters a_1 and f_1 are chosen by the methods which is introduced in the 3.2 section.

The modified transmission signal vector s_g can be expressed as:

$$s_g = G_{doppler} s = a_0 s + a_1 \Delta^{f_1} s \tag{3.2}$$

The modified transmission signal $s_g(t)$ is equivalent to that $s(t)$ be scaled by a_0 and be added to a 'modulated' version of $s(t)$, where the modulation carrier has gain a_1 and frequency f_1. This 'modulated' version of $s(t)$ affects the transmitted signal in the same way as multiplying the original signal by a complex exponential wave. The troughs of this exponential waveform interact with the peaks of the original transmitted signal, effectively canceling them out. This cancellation reduces the overall PAPR, improving

doi:10.6342/NTU202402900

the efficiency and performance of the transmission system.

In Delay-Doppler domain, the modulation carrier is equivalent to a Doppler frequency located at f_1. The modified transmission signal can be seen as shifting f_1 in Doppler frequency. As a result, we name this kind of complex exponential window as Doppler shift window in this thesis.

By examining the following images, where we plot the absolute values of the entire OTFS symbol, we can gain a clearer and more intuitive understanding of the effect of the Doppler shift window in the delay-Doppler domain. First, as shown in Figure 3.1, we place an impulse signal of $1 + 1j$ at the position $(l = 1, k = 1)$. After applying a Doppler shift window with parameters set to $a_1 = 0.5$ and $f_1 = 3$, we can observe in Figure 3.2 that a superimposed signal with a smaller gain appears at the position $(l = 1, k = 4)$. This superimposed signal is the original signal shifted by 3 units in the Doppler dimension. Through this delay-Doppler domain diagram, we can clearly see the response of the Doppler shift window.

doi:10.6342/NTU202402900

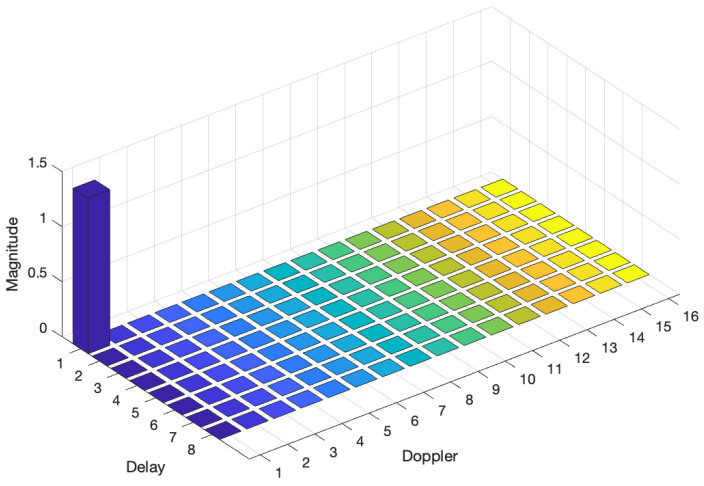

Figure 3.1 Input impulse in Delay doppler domain

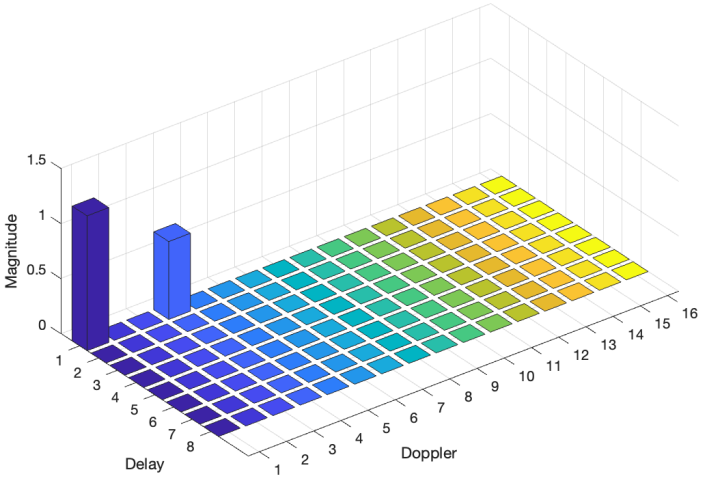

Figure 3.2 an example of Doppler shift window response in Delay Doppler domain

For the receiver, the effect of the window can be merged in the channel response. The equivalent channel response can also be represented as:

$$\mathrm{H}_g = \mathrm{H}G_{doppler} = (\sum_{i=1}^{L} h_i \Pi^{l_i} \Delta^{k_i})(a_0 I_{MN} + a_1 \Delta^{f_1}) \quad (3.3)$$

doi:10.6342/NTU202402900

$$= \sum_{i=1}^{L} a_0 h_i \Pi^{l_i} \Delta^{k_i} + \sum_{i=1}^{L} a_1 h_i \Pi^{l_i} \Delta^{k_i + f_1} \quad (3.4)$$

Since the effect of the window is equal to adding a Doppler shift frequency f_1 to the transmission signal, it can be regarded as additional channel paths in the Doppler domain. For the original channel response with L paths, the equivalent channel response will have $2L$ paths.

In other words, the PAPR reduction introduced by the proposed window method is equal to a modification to the channel response and can be equalized along with the original channel response in the receiver. Now, the scalars a_0, a_1 and the frequency f_1 are the parameters of the equivalent channel response H_g that can evaluated using channel estimation techniques without any side information.

3.1.2 Time delay window

We propose a kind of window G_{delay} called Time delay window which is multiplied to the transmitted signal vector s in time domain to reduce PAPR.

The Time delay window can be expressed in matrix form as follows:

$$G_{delay} = a_0 I_{MN} + a_1 \Pi^{\tau} \quad (3.5)$$

Here $a_0 = \sqrt{(1 - \|a_1\|^2)}$, and the parameters a_1 and τ are selected using the methods introduced in the 3.2 section.

The modified transmission signal vector s_g is given by:

doi:10.6342/NTU202402900

$$s_g = G_{delay}s = a_0 s + a_1 \Pi^{\tau} s \quad (3.6)$$

The modified transmission signal $s_g(t)$ is equivalent to that $s(t)$ be scaled by a_0 and be added to a 'delayed' version of $s(t)$, where the delay signal has gain a_1 and τ-step cyclic shift in the transmitted signal.

To reduce PAPR, the method involves using the destructive interference between the original signal and a delayed version of the signal. This interference helps to cancel out the signal peaks, thereby lowering the overall PAPR. Consequently, this type of window is called as Time delay window in this thesis.

The images below illustrate the absolute values of the entire OTFS symbol, allowing us to more clearly and intuitively understand the effect of the time delay window in the delay-Doppler domain. Similarly, as in Figure 3.1, we only place an impulse signal of $1 + 1j$ at the position $(l = 1, k = 1)$ in the whole OTFS symbol. By applying a time delay window with a gain parameter of $a_1 = 0.5$ and a $\tau = 3$ step cyclic shift, Figure 3.3 reveals a superimposed signal with a reduced gain at the position $(l = 4, k = 1)$. This superimposed signal represents the original signal shifted by 3 units in the delay dimension. The Delay-Doppler domain diagram provides a clear visualization of the time delay window's response.

doi:10.6342/NTU202402900

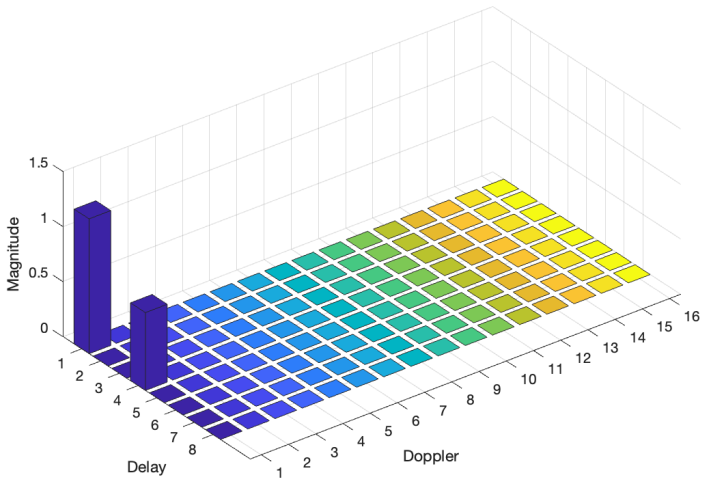

Figure 3.3 an example of Time delay window response in Delay Doppler domain

In essence, the PAPR reduction achieved by the proposed window method corresponds to an adjustment of the channel response and can be aligned with the original channel response during reception.

The equivalent channel response can also be represented in the following manner:

$$\mathrm{H}_g = \mathrm{H}G_{delay} = (\sum_{i=1}^{L} h_i \Pi^{l_i} \Delta^{k_i})(a_0 I_{MN} + a_1 \Pi^{\tau}) \quad (3.7)$$

$$= \sum_{i=1}^{L} a_0 h_i \Pi^{l_i} \Delta^{k_i} + \sum_{i=1}^{L} a_1 h_i \Pi^{l_i+\tau} \Delta^{k_i} \quad (3.8)$$

For an initial channel response with L paths, the resulting equivalent channel response will contain $2L$ paths.

Consequently, the scalars a_0, a_1 along with the cyclic shift steps τ, serve as parameters of the equivalent channel response H_g, which can be determined using channel estimation techniques without requiring any additional side information.

doi:10.6342/NTU202402900

3.1.3 Complex window

By integrating the two previously discussed windowing methods that effectively reduce PAPR, we introduce a composite window described as the Complex window in this thesis.

The underlying principle capitalizes on the effects of both Doppler shift and delay. Through the utilization of the troughs of the added exponential waveform and the low points of the delayed transmission signal, they interact with the peaks of the original transmitted signal, inducing destructive interference. This interference results in a reduction of the PAPR.

The complex window, like the previous windows, is also multiplied with the original transmission signal in the time domain. The design of the complex window resembles the channel effects mentioned earlier. Therefore, we represent it in matrix form as:

$$G_{complex} = a_0 I_{MN} + a_1 \Pi^{\tau} \Delta^{f_1} \quad (3.9)$$

where $a_0 = \sqrt{(1 - \|a_1\|^2)}$, and the parameters a_1, f_1 and τ are selected using the methods described in the 3.2 section.

Next, we can mathematically represent the modified transmitted signal vector s_g as:

$$s_g = G_{complex} s = a_0 s + a_1 \Pi^{\tau} \Delta^{f_1} s \quad (3.10)$$

The modified transmission signal $s_g(t)$ is equivalent to scaling $s(t)$ by a_0 and adding

doi:10.6342/NTU202402900

a ‘modulated’ and ‘delayed’ version of $s(t)$. In this version, the signal has a gain a_1 and τ-step cyclic shift delay in the transmitted signal, while being multiplied by a complex exponential wave modulated by frequency f_1.

Similarly, by plotting the absolute values of the entire OTFS symbol, we can more clearly and intuitively observe the effect of a complex window in the delay-Doppler domain. In Figure 3.1, we place an impulse signal of $1 + 1\text{j}$ at the position $(l = 1, k = 1)$. After applying a complex window with parameters set to a gain of $a_1 = 0.5$, a cyclic shift step of $\tau = 3$, and a Doppler shift frequency of $f_1 = 2$, Figure 3.4 shows a superimposed signal with a smaller gain at the position $(l = 4, k = 3)$. This superimposed signal is the original signal shifted by 3 units in the time delay dimension and 2 units in the Doppler dimension. This delay-Doppler domain diagram clearly illustrates the response of the complex window.

doi:10.6342/NTU202402900

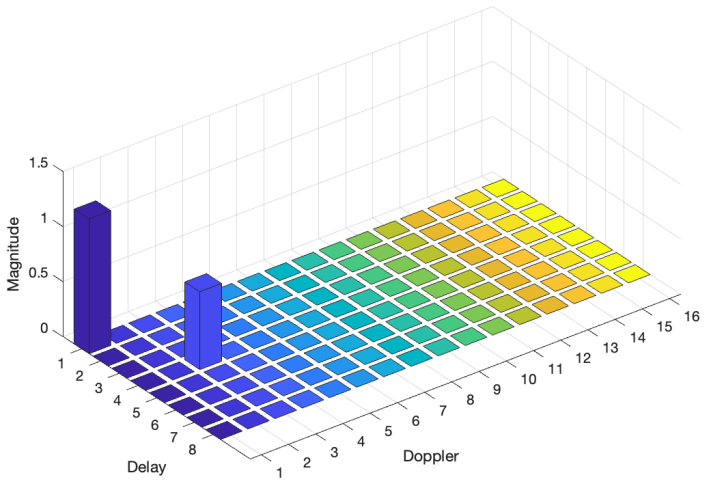

Figure 3.4 an example of Complex window response in Delay Doppler domain

Essentially, the reduction in PAPR attained through the proposed window technique involves fine-tuning the channel response, which can be realigned with the initial channel response at the receiver. This adjusted channel response can alternatively be expressed as follows:

$$\mathrm{H}_g = \mathrm{H}G_{complex} = (\sum_{i=1}^{L} h_i \Pi^{l_i} \Delta^{k_i})(a_0 I_{MN} + a_1 \Pi^{\tau} \Delta^{f_1}) \quad (3.11)$$

$$= \sum_{i=1}^{L} a_0 h_i \Pi^{l_i} \Delta^{k_i} + \sum_{i=1}^{L} a_1 h_i \Pi^{l_i+\tau} \Delta^{k_i+f_1} \quad (3.12)$$

The initial channel response, comprising L paths, will give rise to an equivalent channel response with $2L$ paths.

Consequently, parameters such as the scalars a_0, a_1, the cyclic shift steps τ, and the doppler shift frequency f_1 act as defining factors for the equivalent channel response H_g. These parameters can be established using channel estimation techniques, eliminating the

doi:10.6342/NTU202402900

need for any supplementary side information.

3.2 Parameters selection

We employ several methods to select multiple sets of parameters for the mentioned window function. For each combination of parameters, we calculate the PAPR of $s_g(t)$ after applying the window to the original signal $s(t)$. The candidate with the smallest PAPR is chosen as the window to be used.

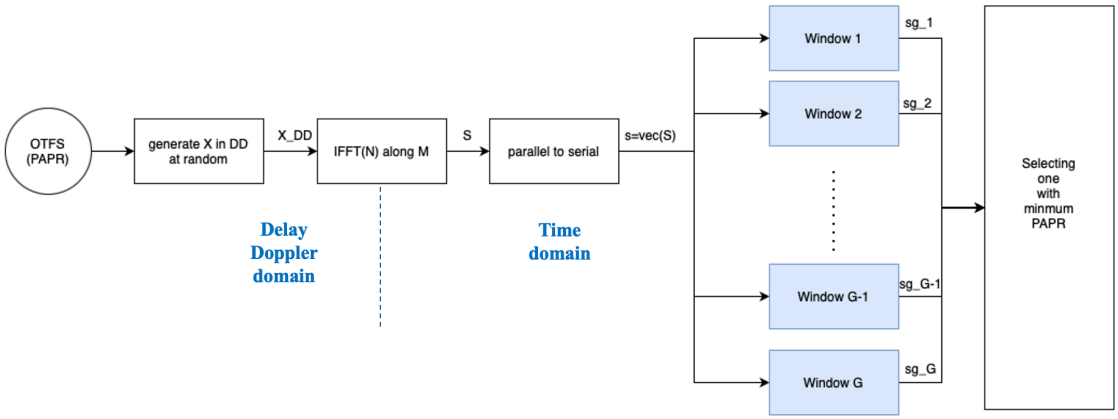

Figure 3.5 the flow diagram of choosing the best window (without oversampling)

doi:10.6342/NTU202402900

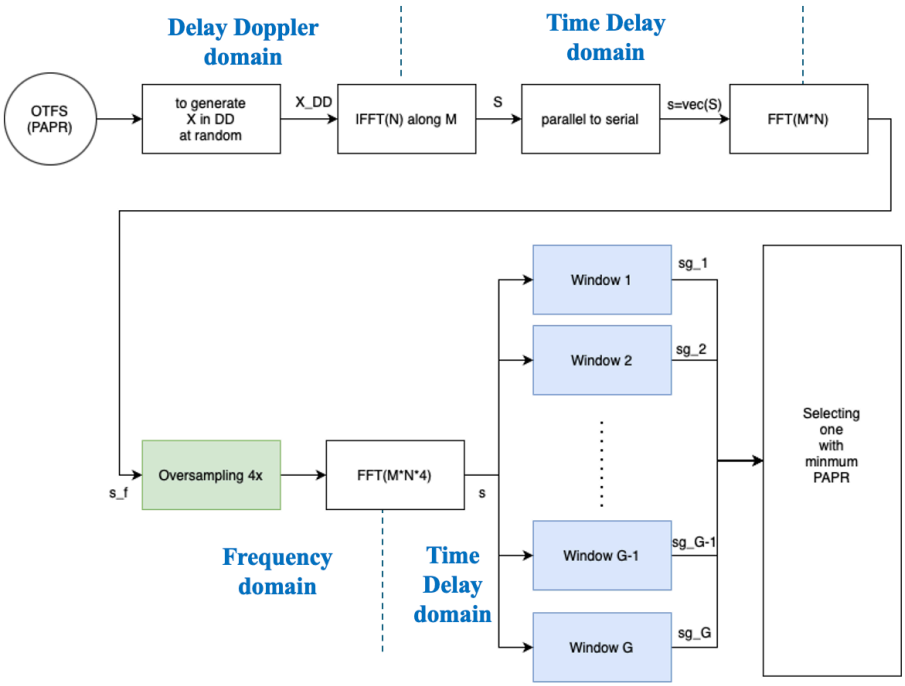

Figure 3.6 the flow diagram of choosing the best window (with oversampling)

We employ several methods to select the parameters in the mentioned window function. These parameters include the gain of window response a_1, which is a complex number, the frequency f_1 that determines the offset for Doppler shift, and the parameter τ that determines the cyclic shift steps for time delay.

The methods for determining these three parameters can be roughly categorized into three types:

1. Random selection method suitable for all types of windows.
2. Parameter derivation method applicable to Doppler shift windows.
3. Grid search method for all combinations within a specified range suitable for all types

doi:10.6342/NTU202402900

of windows.

Notably, the parameter derivation method for Doppler shift windows can be combined with the grid search method for enhanced effectiveness.

3.2.1 Random selection method

The Random Selection Method can be used to preliminarily and simply try out some parameter combinations, aiding in the first step of verifying the feasibility of reducing PAPR with a window and roughly estimating the increase in error rate.

For the Doppler shift window, the parameters that need to be determined are the gain of window response a_1 and the shift frequency f_1. Among these parameters, the gain of window response a_1 is a complex number represented as $ae^{j\theta}$, where a is the magnitude of a_1 and θ is the phase angle of a_1.

The parameters magnitude a, the phase angle θ, and the shift frequency f_1 are determined using the $randn(1)$ function in MATLAB. This function generates a single sample from a standard normal distribution (Gaussian distribution) with a mean of 0 and a standard deviation of 1. Specifically, the magnitude a is given by $0.4 \times randn(1)$, meaning it is derived from a standard normal distribution scaled by 0.4. Consequently, a has a normal distribution with a mean of 0 and a standard deviation of

doi:10.6342/NTU202402900

0.4. The phase angle θ and the shift frequency f_1 are both given by $randn(1)$, indicating that each follows a standard normal distribution with a mean of 0 and a standard deviation of 1.

As for the Time delay window, the parameters that need to be determined are similar, which are the gain of window response a_1 and the cyclic shift step τ. Similarly, the gain of window response a_1 is a complex number represented as $ae^{j\theta}$, where a is the magnitude of a_1 and θ is the phase angle of a_1.

The parameters magnitude a and the phase angle θ are also determined using the $randn(1)$ function in MATLAB. This function generates a single sample from a standard normal distribution (Gaussian distribution) with a mean of 0 and a standard deviation of 1. Specifically, the magnitude a is given by $0.4 \times randn(1)$, meaning it is derived from a standard normal distribution scaled by 0.4. Consequently, a has a normal distribution with a mean of 0 and a standard deviation of 0.4. The phase angle θ is given by $randn(1)$, indicating that each follows a standard normal distribution with a mean of 0 and a standard deviation of 1.

Here, we should notice that the cyclic shift step τ is determined using the $randi(3)$ function in MATLAB, which gives a discrete uniform distribution over the integers 1, 2, and 3. The parameters have the mean $\mu_\tau = 2$ and the standard deviation $\sigma_\tau = 0.8165$.

doi:10.6342/NTU202402900

The reason why the cyclic shift step τ must be an integer is that only integer cyclic shift steps can be effectively sampled and manifested when signals are combined. This ensures the shifted signals align correctly with the sampling process, accurately reflecting the desired delay effect.

For summary, using the Random Selection Method, we can effectively sample various parameter combinations. This helps in assessing the feasibility of reducing PAPR and understanding the potential impact on error rates in the initial verification phase.

3.2.2 Parameter derivation method for Doppler shift window

The parameter derivation method for the Doppler Shift Window allows for a rough estimation of suitable parameters, which can later be optimized using grid search to further reduce the Peak-to-Average Power Ratio.

The Doppler Shift Window requires the determination of two parameters: the gain of window response a_1, which is a complex number with both amplitude and phase components, and the frequency f_1 that determines the offset for the Doppler shift. This method primarily utilizes the indices of the peak powers of the original transmission signal to determine these parameters.

To begin with, the first step involves identifying the sample time T_p, where the first largest power of the transmission signal is located. Following this, one must determine T_Δ

doi:10.6342/NTU202402900

, which represents the number of samples between the first and second largest power peaks. Using this information, the frequency f_1 can be calculated as :

$$f_1 = \frac{1}{T_\Delta} \quad (3.13)$$

Next, the phase of the gain a_1 is determined using the formula:

$$\arg(a_1) = \pi - \frac{2\pi}{MN} f_1 T_p \quad (3.14)$$

where M and N are constants related to the system configuration.

The maximum amplitude $\|a_1\|$ of the complex exponential window can then be set according to the equation:

$$\|a_1\| = \alpha\left(1 - \frac{E[|x(t)|^2]}{max|x(t)|}\right) \quad (3.15)$$

Here, α is a scaling factor. When $\alpha = 1$, the complex exponential window is expected to mitigate the original peak power to the same level as the average power. However, based on empirical tests, the scale α is usually set between 0.2 and 0.5 to reduce unwanted amplification of the signals between the first and second peak powers. In this thesis, we set $\alpha = 0.4$ for all simulations.

From Figure 3.7, it can be observed that the window function derived from these parameters forms a complex exponential wave with its troughs aligned with the peaks of the original signal. This alignment effectively reduces PAPR when the window function is applied. Although this method provides a rough estimation of the parameters and may

doi:10.6342/NTU202402900

not yield the optimal solution, it serves as a foundation. Further optimization can be achieved using the grid search method, which helps refine the parameter search range and reduces the number of combinations to be tested. By doing so, the complexity of finding better window parameter combinations is lowered, leading to more effective PAPR reduction with less computational effort.

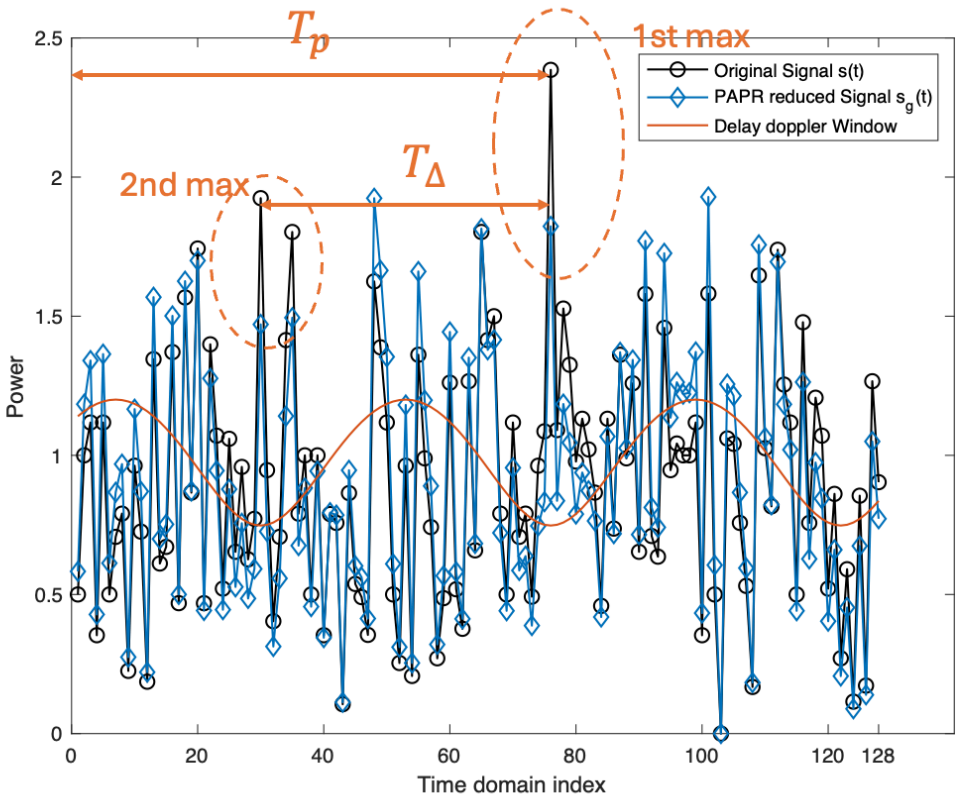

Figure 3.7 an example of PAPR reduction using Doppler shift window

3.2.3 Grid search method

The grid search method aims to find the parameter combination that minimizes the

doi:10.6342/NTU202402900

Peak-to-Average Power Ratio when a window is applied to the original signal. This systematic approach is suitable for all types of windows and involves determining up to four parameters. The choice of parameters depends on the window type, allowing for a tailored optimization approach.

Among these parameters, a_1 is a complex number whose amplitude and phase angle are respectively named $scal\_idx$ and ang_idx. The frequency determining the offset of the Doppler shift, f_1, is referred to as dop_idx. The parameter τ, which determines the cyclic shift steps for the time delay, is named dly_idx.

To achieve this goal, the grid search method involves several key steps. First, it begins by defining a discrete set of possible values for each parameter. These ranges can be based on empirical tests or theoretical considerations. Once the ranges are established, each parameter range is divided into a finite number of discrete points, forming a grid. This grid represents all possible combinations of parameter values.

Next, the method involves systematically evaluating each combination of parameters on the grid. For each combination, the corresponding window function is applied to the original signal, and the PAPR is calculated. The objective is to find the parameter combination that results in the lowest PAPR.

The primary benefits of the grid search method is its exhaustive search capability.

doi:10.6342/NTU202402900

By systematically exploring all possible combinations of parameters within the defined ranges, grid search increases the likelihood of finding the global optimum. This thorough exploration ensures that no potential solution is overlooked.

Despite its benefits, the grid search method also has the drawback. The primary disadvantage is its computational expense. As the number of parameters and the range of values increase, the number of combinations grows exponentially. This leads to a significant increase in computational time and resources, making grid search less efficient for high-dimensional parameter spaces.

doi:10.6342/NTU202402900

Chapter 4 Numerical Results

In this section, we organize simulations into two main parts: section 4.1 simulations without oversampling and section 4.2 simulations with oversampling. The reason for this is that, without oversampling, the system's computational complexity is lower. This allows us to easily try various parameter selection methods, numerous parameter combinations, and conduct preliminary tests on the effects of the three types of windows. Based on the initial experimental results from the first part, we then apply the windows to the system with oversampling, aiming to achieve better parameter combinations and results.

4.1 Simulations without oversampling

4.1.1 Parameter setting in common use

The simulations in this thesis utilize an OTFS framework with parameters $M = 8$ for delays and $N = 16$ for Dopplers. This configuration allows for the transmission of $8 \times 16 = 128$ signals within each frame in the Delay-Doppler (DD) domain. Each symbol in the DD domain, denoted as $X_{DD}[l, k]$, is mapped to the Quadrature Phase Shift Keying (QPSK) constellation. The transmission channels employed in the simulations is

doi:10.6342/NTU202402900

a three path Rayleigh fading channel. Additive White Gaussian Noise (AWGN) is added to the signal in all simulations to assess performance. In this section, all simulations for calculating PAPR were collected using 10,000 blocks, while the bit error rate was determined by collecting data from 10^7 blocks.

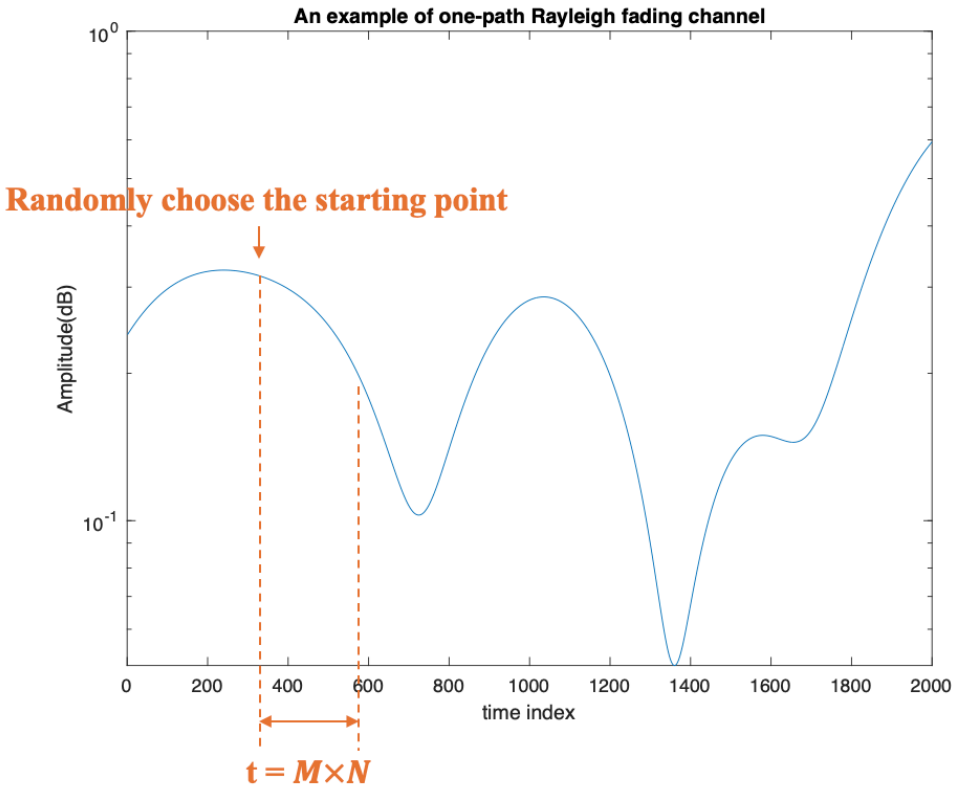

Figure 4.1 an example of one-path Rayleigh fading channel in time domain

4.1.2 Grid search range for Doppler shift window

For the Doppler shift window, the parameters that need to be determined are the gain of window response a_1 and the shift frequency f_1. The gain of window response a_1 is a complex number characterized by its amplitude, referred to as $scal\_idx$, and its phase

doi:10.6342/NTU202402900

angle, referred to as ang_idx. The shift frequency f_1, which determines the offset for the Doppler shift, is referred to as dop_idx.

The methods for determining the Doppler shift window parameters can be categorized into four types: random selection, parameter derivation, grid search, and a combination of parameter derivation and grid search. The random selection and parameter derivation methods have been introduced in the previous chapter, so this section will focus on the parameter settings for the grid search method.

In the grid search method, each parameter is varied within a specified range to find the optimal combination.

For the combination of derived parameters with grid search, the following settings are used:

For the amplitude $scal\_idx$, if the derived parameter is $scal\_d$, the range is set from $scal\_d - 3$ to $scal\_d + 3$ with an increment of 1, resulting in a total of 7 values.

For the phase angle ang_idx, if the derived parameter is ang_d, the range is set from $ang\_d + \frac{1}{16}\pi$ to $ang\_d + 2\pi$ with an increment of $\frac{1}{16}\pi$, resulting in a total of 32 values.

For the Doppler shift frequency dop_idx, if the derived parameter is dop_d, the range is set from $dop\_d + 1$ to $dop\_d + 3$ with an increment of 1, resulting in a total of

doi:10.6342/NTU202402900

3 values.

Combining these ranges, the total number of combinations for the derivation and grid search method is $7 \times 32 \times 3 = 672$ combinations.

For the grid search ranges of Doppler shift window are set as follows:

For the amplitude $scal\_idx$, the range is set from 0.05 to 0.5 with an increment of 0.05, resulting in a total of 10 values.

For the phase angle ang_idx, the range is set from $\frac{1}{16}\pi$ to 2π with an increment of $\frac{1}{16}\pi$, resulting in a total of 32 values.

For the Doppler shift frequency dop_idx, the range is set from 1 to 10 with an increment of 1, resulting in a total of 10 values.

Combining these ranges, the total number of combinations for the grid search method is $10 \times 32 \times 10 = 3200$ combinations. This comprehensive approach allows for a thorough exploration of the parameter space to optimize the Doppler shift window's performance.

4.1.3 Grid search range for time delay window

For the Time delay window, the parameters that need to be determined are similar to those for the Doppler shift window: the gain of window response a_1 and the cyclic shift step τ. Specifically, a_1 is a complex number characterized by its amplitude, referred to

doi:10.6342/NTU202402900

as $scal\_idx$, and its phase angle, referred to as ang_idx. The parameter τ, determining the cyclic shift steps for the time delay, is denoted as dly_idx.

There are two main methods for determining the Time delay window parameters: random selection and grid search. While the random selection method has been discussed in the previous chapter, this section focuses on detailing the parameter settings for the grid search method.

The grid search method involves systematically varying each parameter within specified ranges to identify the optimal combination. The ranges for the Time delay window parameters in the grid search method are as follows:

The amplitude $scal\_idx$ ranges from 0.05 to 0.5, with increments of 0.05, yielding a total of 10 values.

The phase angle ang_idx spans from $\frac{1}{16}\pi$ to 2π, with increments of $\frac{1}{16}\pi$, resulting in 32 values.

The cyclic shift step dly_idx extends from 1 to 10, with increments of 1, giving 10 values.

When combining these ranges, the total number of parameter combinations for the grid search method is calculated as $10 \times 32 \times 10 = 3200$ combinations. This thorough exploration of the parameter space is essential for optimizing the performance of the Time

doi:10.6342/NTU202402900

delay window.

4.1.4 Grid search range for complex window

For the complex window, four parameters need to be determined: The gain of window response a_1 is a complex number characterized by its amplitude, referred to as $scal\_idx$, and its phase angle, referred to as ang_idx. The frequency determining the offset of the Doppler shift f_1 is denoted as dop_idx. The parameter τ, which determines the cyclic shift steps for the time delay, is referred to as dly_idx.

To find the optimal combination of these parameters, we use the grid search method. The parameter settings for the grid search method are as follows:

The amplitude $scal\_idx$ ranges from 0.05 to 0.6 with increments of 0.05, resulting in a total of 14 values.

The phase angle ang_idx spans from $\frac{1}{16}\pi$ to 2π with increments of $\frac{1}{16}\pi$, resulting in a toral 32 values.

The Doppler shift frequency dop_idx, the range is set from 1 to 3 with an increment of 1, resulting in a total of 3 values.

The cyclic shift step dly_idx extends from 1 to 3, with increments of 1, giving 3 values.

By combining these ranges, the total number of parameter combinations for the grid

doi:10.6342/NTU202402900

search method is calculated as $14 \times 32 \times 3 \times 3 = 4032$ combinations.

This extensive grid search allows for a comprehensive exploration of the parameter space, aiming to optimize the performance of the complex window.

4.1.5 The simulation result of Doppler shift window

The results of PAPR reduction for different sets of Doppler shift window parameters chosen using the random selection method are demonstrated in Figure 4.2.

The blue curve represents the CCDF of the PAPR for the original signal without any window applied. This curve serves as a baseline for comparison with the other curves. The other curves represent the PAPR results after applying the Doppler shift window with parameters chosen using random selection. All random selection scenarios (10, 50, and 1000 candidates) show improved PAPR reduction compared to the original signal. This demonstrates the effectiveness of the Doppler shift window in reducing PAPR.

The results clearly show that as the number of random candidates increases, the PAPR reduction becomes more significant. This is because a larger pool of random candidates increases the likelihood of finding a more optimal parameter set.

There is a noticeable trade-off between the computational effort and the performance of the PAPR reduction. While evaluating more candidates results in better PAPR reduction, it also requires more computational resources and time.

doi:10.6342/NTU202402900

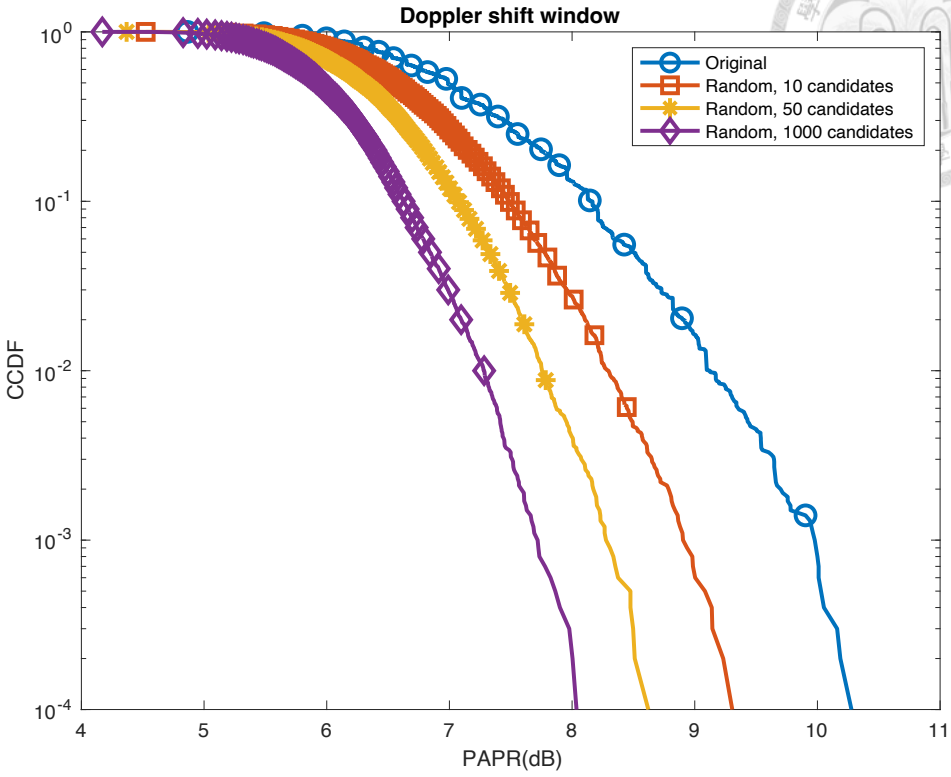

Figure 4.2 The CCDF curves of PAPR reduction using Doppler shift window selected parameters randomly with different amount of candidates

The results of PAPR reduction for different sets of Doppler shift window parameters chosen using the parameter derivation method and grid search method are demonstrated in Figure 4.3.

The orange square curve shows the PAPR results when using parameters derived from the indices of the peak powers of the original transmission signal. This method reduces the PAPR compared to the original signal, indicating the effectiveness of the derived parameters in lowering the PAPR. However, it may not yield the optimal results.

doi:10.6342/NTU202402900

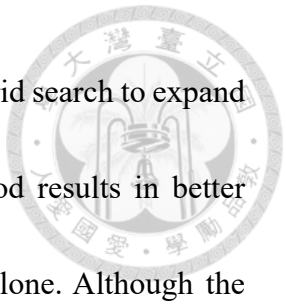

According to the yellow star curves, we can observe that using grid search to expand the parameter search range based on the derived parameters method results in better performance compared to using the parameter derivation method alone. Although the effect is not as good as the purple diamond curve, which uses the grid search method with 3200 combinations, the approach based on derived parameters only requires a grid search with 672 combinations. This significantly reduces computational complexity and time. The purple diamond curve shows the best PAPR reduction effect. However, this grid search method requires trying a total of 3200 parameter combinations. Although the effect is the best, we must also consider the trade-off between computational complexity and time.

doi:10.6342/NTU202402900

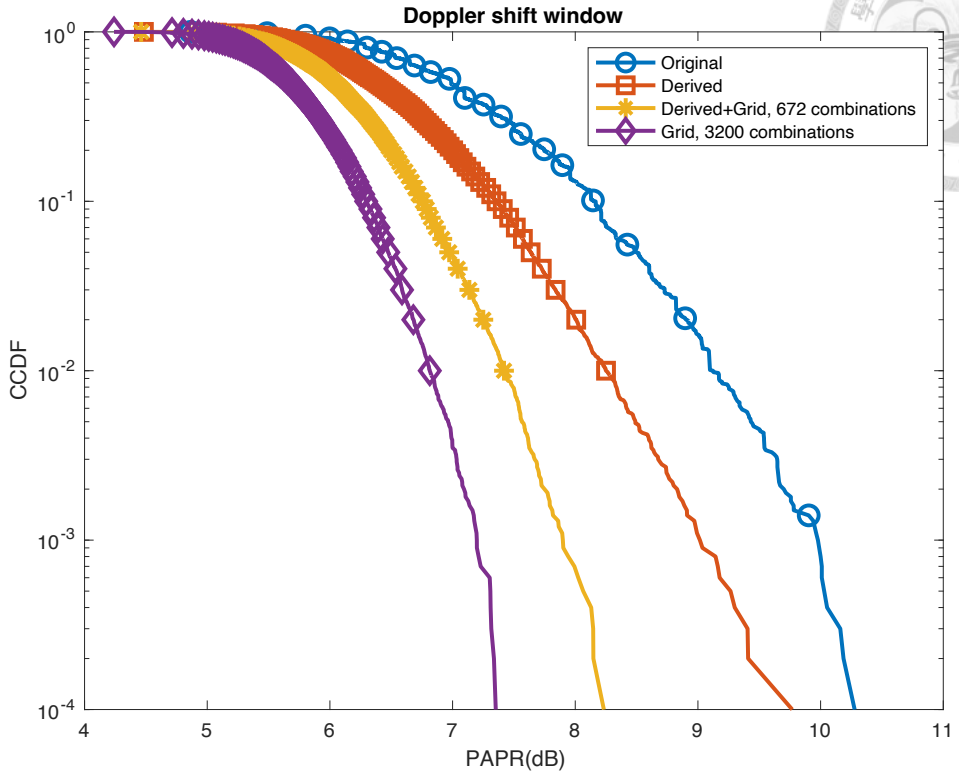

Figure 4.3 The CCDF curves of PAPR reduction using Doppler shift window whose parameters chosen by the derivation method and grid search method

The Figure 4.4 compares various methods for reducing the Peak-to-Average Power Ratio (PAPR) using different parameter selection techniques for Doppler shift windows.

The orange square curve show that derived parameters method alone provides a substantial reduction in PAPR, serving as a good starting point. Then, according to the yellow star curve, the combination of derived parameters with grid search (672 combinations) enhances the PAPR reduction further, indicating that a focused search based on derived parameters can be very effective and efficient.

doi:10.6342/NTU202402900

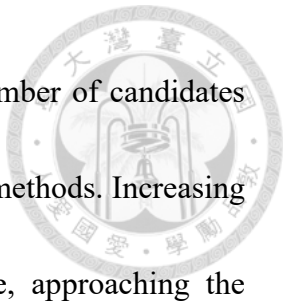

We can observe that using random selection with a limited number of candidates provides some PAPR reduction but is less effective than grid search methods. Increasing the number of random candidates to 1000 improves performance, approaching the effectiveness of the derived parameters combined with grid search method (672 combinations).

The light blue diamond curve shows the grid search with 3200 combinations achieves the best PAPR reduction, showcasing the benefit of an exhaustive search. However, the computational complexity and time required for this method are significantly higher.

In conclusion, this comprehensive plot highlights that combining derived parameters with a focused grid search offers an efficient and effective method for PAPR reduction. It achieves a good balance between performance and computational cost. While exhaustive grid searches provide the best results, they require substantial computational resources, making them less practical for real-time applications. Random selection methods offer flexible alternatives with varying performance based on the candidate pool size.

doi:10.6342/NTU202402900

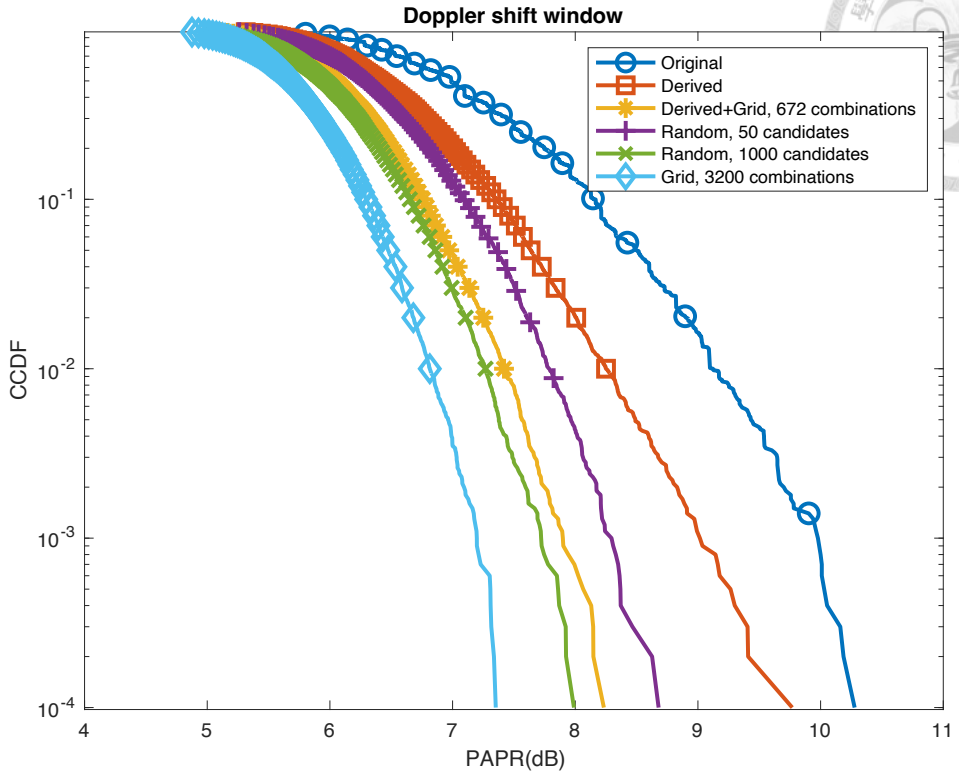

Figure 4.4 The CCDF curves of PAPR reduction using Doppler shift window whose parameters chosen by different methods

Here is an analysis of the bit error rate (BER) result Figure 4.5, which compares the performance of different methods for selecting Doppler shift window parameters.

The random selection method for window parameters serves primarily as an initial test to determine whether the window can effectively reduce PAPR. Therefore, when calculating the bit error rate, the random selection method is not included.

This blue circle curve serves as the reference, showing the best BER performance as no window is applied.

doi:10.6342/NTU202402900

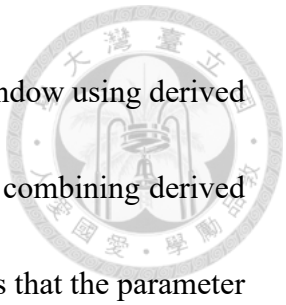

The orange cross curve is the BER result of the Doppler shift window using derived parameters. The yellow star curve represents the BER of the method combining derived parameters with grid search using 672 combinations. We can observes that the parameter derivation method slightly optimizes BER performance than the combination method.

The purple triangle curve shows the BER result of the method using grid search with 3200 combinations. While this method offers the best PAPR reduction, it has a slightly higher BER compared to the parameter derivation method and the combination of derivation and grid search method. This suggests a trade-off between PAPR reduction and BER performance.

doi:10.6342/NTU202402900

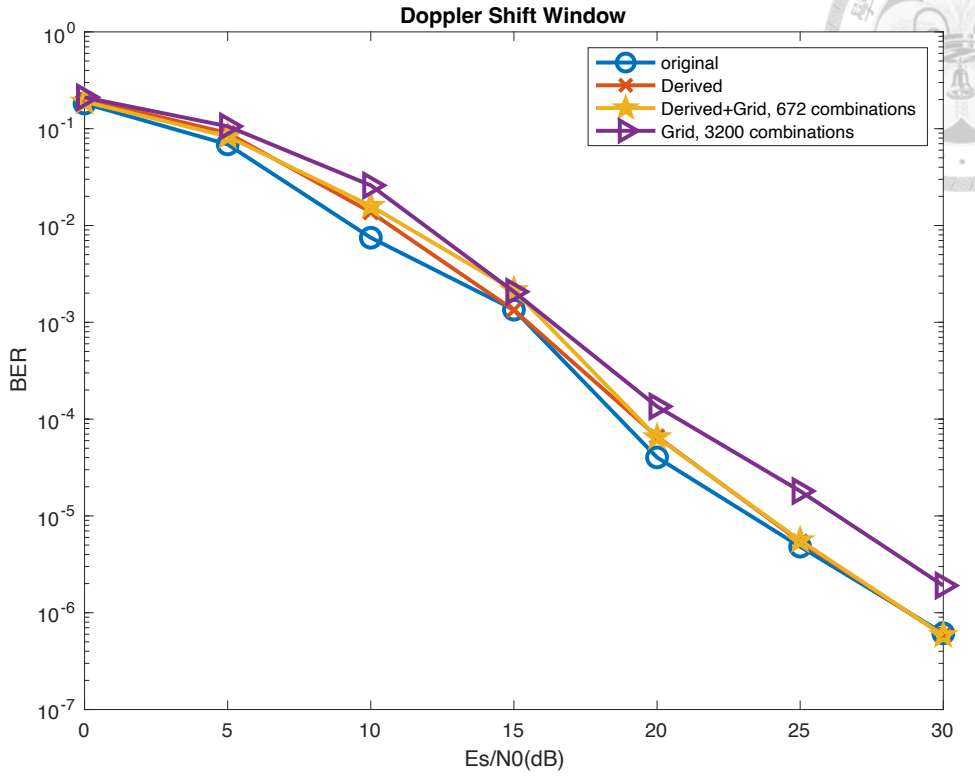

Figure 4.5 The BER curves of Doppler shift window whose parameters chosen by derivation and grid search methods

4.1.6 The simulation result of Time delay window

The Figure 4.6 compares random and grid search methods for selecting time delay window parameters to reduce the PAPR.

The blue circle curve serves as the baseline, showing the PAPR distribution of the signal without any window applied. This orange curve shows the PAPR results when using the random selection method with 10 candidates. There is a noticeable improvement in PAPR reduction compared to the original signal, indicating the effectiveness of even a

doi:10.6342/NTU202402900

small random search. Increasing the number of random candidates to 50 further reduces the PAPR. The yellow star curve shifts leftward compared to the 10 candidates method, demonstrating that evaluating more candidates improves the chances of finding better parameters. The random selection method shows a clear trend: as the number of candidates increases, the PAPR reduction improves.

This purple diamond curve represents the PAPR results when using an extensive grid search with 3200 different combinations of parameters. This grid search method achieves the best PAPR reduction, demonstrating the most substantial leftward shift. The grid search method thoroughly explores the parameter space, resulting in the lowest PAPR values among all evaluated methods. However, it markes the grid search method as the most effective but also the most computationally intensive.

In conclusion, this figure illustrates that both random selection and grid search methods effectively reduce PAPR. The grid search method yields the best results but at a high computational cost.

doi:10.6342/NTU202402900

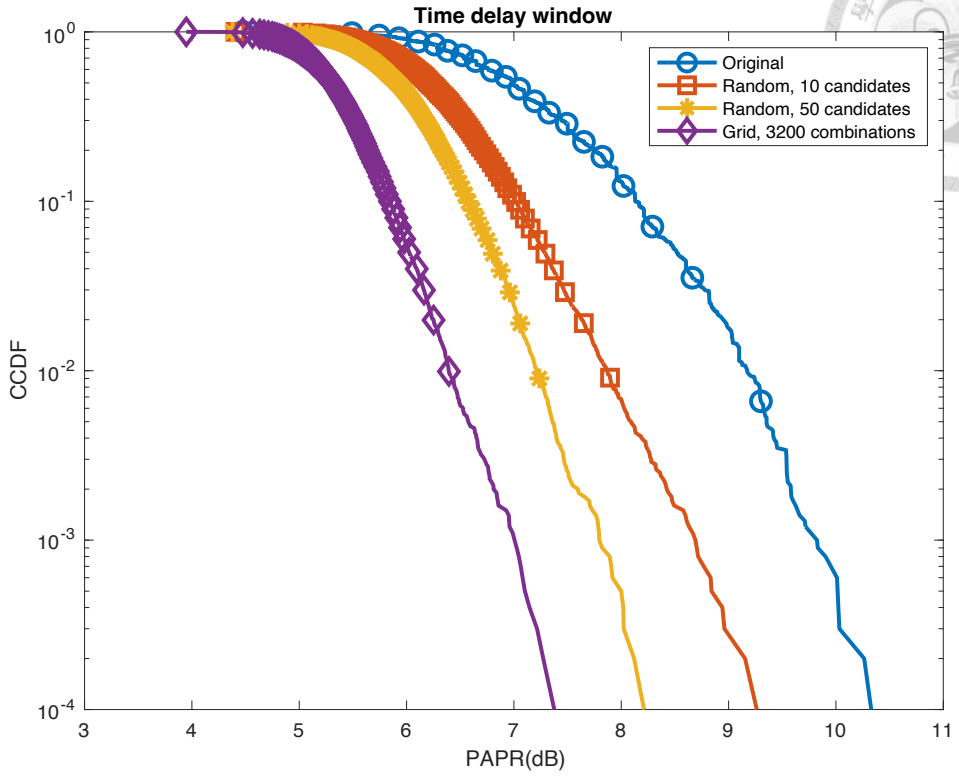

Figure 4.6 The CCDF curves of PAPR reduction using time delay window whose parameters chosen by different methods

The random selection method for window parameters is initially used to test if applying a window can effectively reduce the Peak-to-Average Power Ratio (PAPR). However, when evaluating the Bit Error Rate (BER), we do not include the random selection method. Instead, we compare the BER results of the original raw data (without any windowing) with those obtained using grid search to find optimal time delay window parameters.

The blue circle curve serves as the reference, showing the best BER performance as

doi:10.6342/NTU202402900

no window is applied. The orange cross curve represents the BER performance of the system where a grid search algorithm is applied to select the time delay window to reduce the PAPR.

Across the SNR range, the original system consistently shows a lower BER compared to the system with the time delay window applied.

While the time delay window aims to reduce PAPR, which is beneficial for improving power efficiency, it appears to have an adverse effect on the BER in this case. This might be due to the inherent trade-offs involved in reducing PAPR at the cost of increased BER.

doi:10.6342/NTU202402900

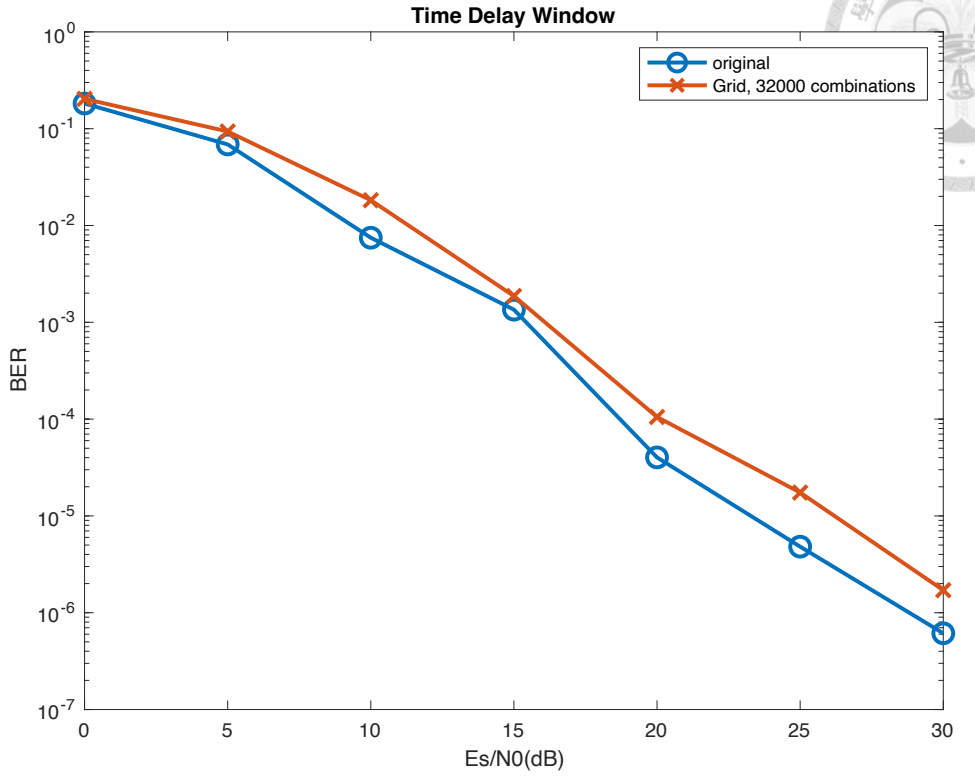

Figure 4.7 The BER curves of time delay window whose parameters chosen by grid search methods

4.1.7 The simulation result of complex window

The Figure 4.8 compares the effectiveness of different methods for reducing the Peak-to-Average Power Ratio (PAPR) using grid search for three window types.

The blue circle curve serves as the baseline, showing the PAPR distribution of the signal without any windowing applied. This orange square curve represents the results of using the grid search method with 3200 combinations for the Doppler shift window parameters. There is a noticeable reduction in PAPR compared to the original signal. The

doi:10.6342/NTU202402900

yellow star curve illustrates the PAPR results for the time delay window using grid search with 3200 combinations. The performance is similar to that of the Doppler shift window, showing a significant reduction in PAPR. By using a grid search with 4032 combinations, the purple diamond curve demonstrates a substantial reduction in PAPR due to the complex window, better than the Doppler shift and time delay windows.

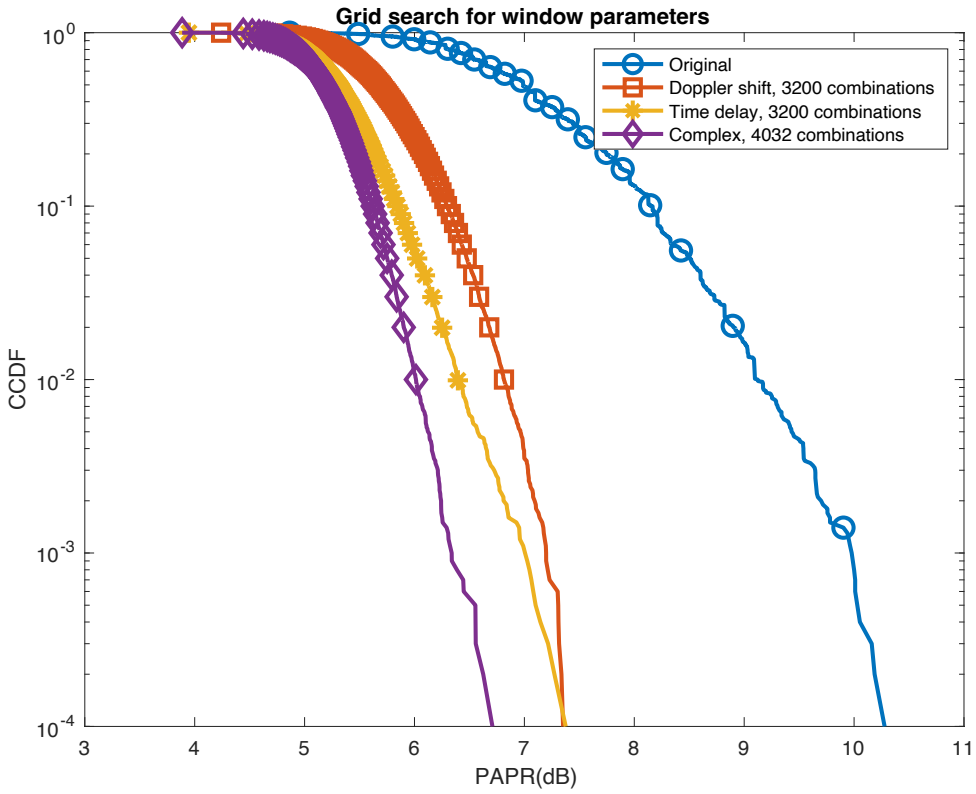

Figure 4.8 The CCDF curves of PAPR reduction using different windows whose parameters chosen by grid search (without oversampling)

According to Figure 4.9, we can observe that the blue circle curve serves as the baseline, showing the BER of the signal without any windowing applied. The orange

doi:10.6342/NTU202402900

triangle curve represents the BER results of using the Doppler shift window, evaluating 3200 combinations of parameters. The yellow cross curve illustrates the BER results for the time delay window using grid search with 3200 combinations. The performance is similar to that of the Doppler shift window. These two methods result in a slight increase in BER compared to the original system but still perform reasonably well.

By using a grid search with 4032 combinations, the purple star curve demonstrates a higher BER than the original system and the system applied the Doppler shift window or time delay window, but the increase in BER is relatively minor. The BER performance is still acceptable, considering the significant benefits in PAPR reduction. However, evaluating 4032 combinations, it indicates a higher computational complexity compared to the 3200 combinations in the other window methods.

In summary, the complex window is the most effective among three types of windows all using grid search for optimal parameter combination due to its significant PAPR reduction and only a minor increase in BER. Despite the higher computational complexity (evaluating 4032 combinations), its benefits in PAPR reduction make it the best choice for applications where both BER and PAPR are critical performance metrics.

doi:10.6342/NTU202402900

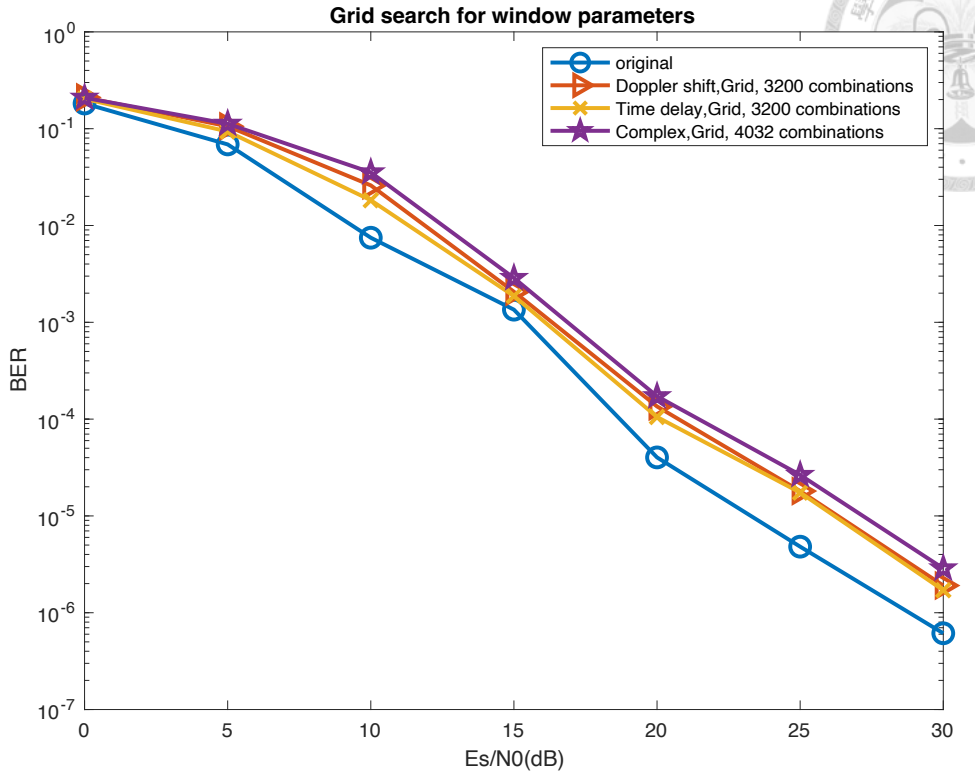

Figure 4.9 The BER curves of different windows whose parameters chosen by grid search (without oversampling)

4.2 Simulations with oversampling

4.2.1 Parameter setting in common use

As the previous section 4.1.1 of simulation without oversampling, the simulations in this thesis utilize an OTFS framework with parameters $M = 8$ for delays and $N = 16$ for Dopplers. In this section, the system undergoes a 4x oversampling process. Apply an oversampling factor of 4, which means each subcarrier (M) and time slot (N) will be sampled four times more than the standard rate. This configuration allows for the

doi:10.6342/NTU202402900

transmission of $8 \times 16 = 128$ signals within each frame in the Delay-Doppler (DD) domain. Each symbol in the DD domain, denoted as $X_{DD}[l,k]$, is mapped to the Quadrature Phase Shift Keying (QPSK) constellation. The transmission channels employed in the simulations is a three path Rayleigh fading channel. Additive White Gaussian Noise (AWGN) is added to the signal in all simulations to assess performance. In this section, all simulations for calculating PAPR were collected using 1000 blocks, while the bit error rate was determined by collecting data from 10^5 blocks.

4.2.2 Grid search range for Doppler shift window

For the Doppler shift window, the parameters that need to be determined are the gain of window response a_1 and the shift frequency f_1. The gain of window response a_1 is a complex number characterized by its amplitude, referred to as $scal\_idx$, and its phase angle, referred to as ang_idx. The shift frequency f_1, which determines the offset for the Doppler shift, is referred to as dop_idx.

For the grid search ranges of Doppler shift window are set as follows:

1. For the amplitude $scal\_idx$, the range is set from 0.1 to 0.5 with an increment of 0.1, resulting in a total of 5 values.
2. For the phase angle ang_idx, the range is set from $\frac{1}{8}\pi$ to 2π with an increment of $\frac{1}{8}\pi$, resulting in a total of 16 values.
3. For the Doppler shift frequency dop_idx, the range is set from 1 to 3 with an increment of 1, resulting in a total of 3 values.

doi:10.6342/NTU202402900

Combining these ranges, the total number of combinations for the grid search method is $5 \times 16 \times 3 = 240$ combinations. This comprehensive approach allows for a thorough exploration of the parameter space to optimize the Doppler shift window's performance.

4.2.3 Grid search range for Time delay window

For the Time delay window, the parameters that need to be determined are similar to those for the Doppler shift window: the gain of window response a_1 and the cyclic shift step τ. Specifically, a_1 is a complex number characterized by its amplitude, referred to as $scal\_idx$, and its phase angle, referred to as ang_idx. The parameter τ, determining the cyclic shift steps for the time delay, is denoted as dly_idx.

The grid search method involves systematically varying each parameter within specified ranges to identify the optimal combination. The ranges for the Time delay window parameters in the grid search method are as follows:

1. The amplitude $scal\_idx$ ranges from 0.1 to 0.5, with increments of 0.1, yielding a total of 5 values.
2. The phase angle ang_idx spans from $\frac{1}{8}\pi$ to 2π, with increments of $\frac{1}{8}\pi$, resulting in 16 values.
3. The cyclic shift step dly_idx extends from 1 to 3, with increments of 1, giving 3 values.

When combining these ranges, the total number of parameter combinations for the

doi:10.6342/NTU202402900

grid search method is calculated as $5 \times 16 \times 3 = 240$ combinations. This thorough exploration of the parameter space is essential for optimizing the performance of the Time delay window.

4.2.4 Grid search range for complex window

For the complex window, four parameters need to be determined: The gain of window response a_1 is a complex number characterized by its amplitude, referred to as $scal\_idx$, and its phase angle, referred to as ang_idx. The frequency determining the offset of the Doppler shift f_1 is denoted as dop_idx. The parameter τ, which determines the cyclic shift steps for the time delay, is referred to as dly_idx.

To find the optimal combination of these parameters, we use the grid search method. The parameter settings for the grid search method are as follows:

1. The amplitude $scal\_idx$ ranges from 0.1 to 0.5 with increments of 0.1, resulting in a total of 5 values.
2. The phase angle ang_idx spans from $\frac{1}{8}\pi$ to 2π with increments of $\frac{1}{8}\pi$, resulting in a toral 16 values.
3. The Doppler shift frequency dop_idx, the range is set from 1 to 3 with an increment of 1, resulting in a total of 3 values.
4. The cyclic shift step dly_idx extends from 1 to 3, with increments of 1, giving 3 values.

doi:10.6342/NTU202402900

By combining these ranges, the total number of parameter combinations for the grid search method is calculated as $5 \times 16 \times 3 \times 3 = 720$ combinations. This extensive grid search allows for a comprehensive exploration of the parameter space, aiming to optimize the performance of the complex window.

4.2.5 The simulation results of windows

This Figure 4.10 presents the PAPR reduction performance after oversampling using four different methods: Doppler shift window, time delay window, complex window, and Mu-law ($\mu = 1.5$). The parameters for each window method were optimized using grid search with a specified number of combinations.

The original signal without any PAPR reduction exhibits the highest PAPR across all the methods tested. This blue circle curve serves as the baseline for comparison.

The Doppler shift window and Time delay window method achieves a notable reduction in PAPR compared to the original signal. However, their performance is slightly inferior to the Mu-law method and the complex window method. This suggests that while effective, it is not the most efficient PAPR reduction technique among those tested.

The green cross curve shows that the Mu-law method with $\mu = 1.5$ performs better than the Doppler shift and time delay window methods but is outperformed by the

doi:10.6342/NTU202402900

complex window method.

The purple diamond curve of complex window method shows the most significant reduction in PAPR, outperforming all other methods, including Mu-law. This demonstrates its superior capability in mitigating PAPR, achieving the lowest PAPR values among the methods tested.

The results emphasize that the complex window method is the most effective for PAPR reduction, making it a superior choice among the methods tested. Moreover, the window-based methods have the advantage that their effects can be incorporated into the channel model and mitigated using MMSE equalization. This integration theoretically ensures that the error rate does not increase significantly, making window-based methods particularly attractive when balancing PAPR reduction and computational complexity.

doi:10.6342/NTU202402900

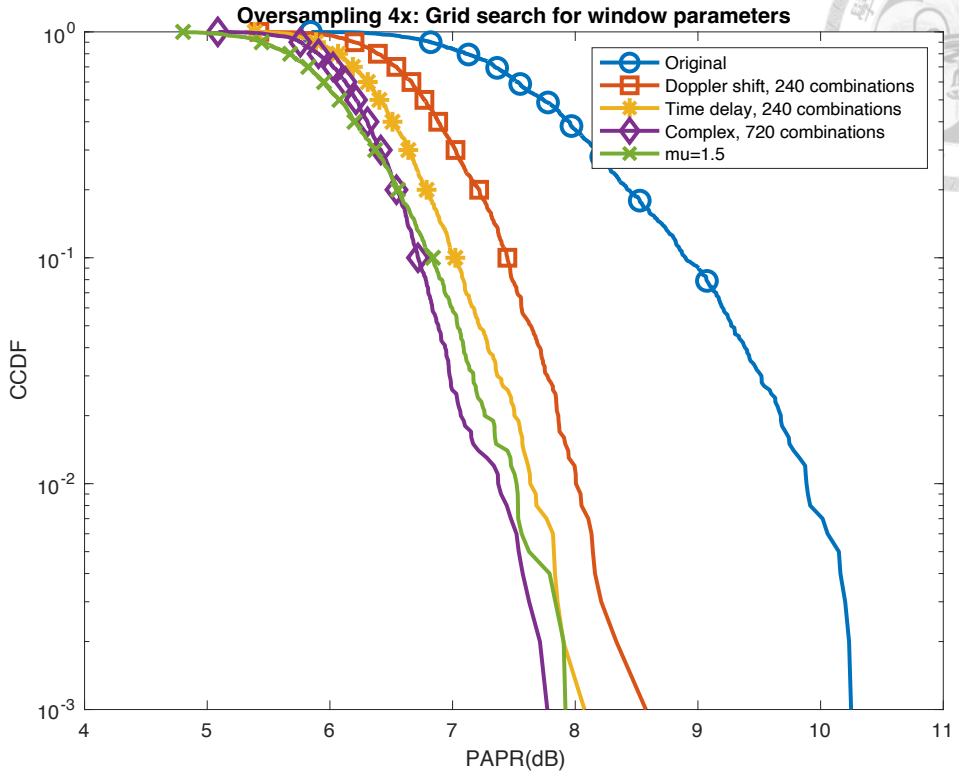

Figure 4.10 The CCDF curves of PAPR reduction using different windows whose parameters chosen by grid search (with oversampling)

The Figure 4.11 illustrates the Bit Error Rate (BER) results after applying oversampling and utilizing the grid search method to determine the parameters for three types of windows (Doppler shift window, time delay window, and complex window), alongside using the mu-law method with $\mu = 1.5$.

The red cross curves shows that mu-law method results in a higher BER compared to other methods across various SNR values. Although the mu-law method shows a good PAPR reduction effect, as indicated in the Figure 4.10, the higher BER indicates that while

doi:10.6342/NTU202402900

it is effective in reducing peak power, it adversely impacts the signal quality more than the other methods.

According to the yellow diamond curve and purple triangle curve, the application of Doppler shift window, with 240 combinations of parameters, shows a comparable BER to the original signal, and it also demonstrates a slightly better BER performance than the time delay window with the same combinations of parameters. Although the BER of the time delay window method is slightly higher than that of the Doppler shift window, its PAPR reduction effect is also better. Therefore, it indicates that the Doppler shift window and time delay window both can balance PAPR reduction and BER performance effectively.

On the other hand, through the green star curve, we can observe that the complex window method shows the highest BER among the three window methods but still performs better than the mu-law technique. Additionally, the complex window achieves the best PAPR reduction among all the methods, including mu-law. These experimental results confirm our hypothesis that windows can be treated as part of the channel and mitigated using MMSE without significantly increasing the BER. This further highlights the effectiveness and advantages of using window techniques for PAPR reduction.

doi:10.6342/NTU202402900

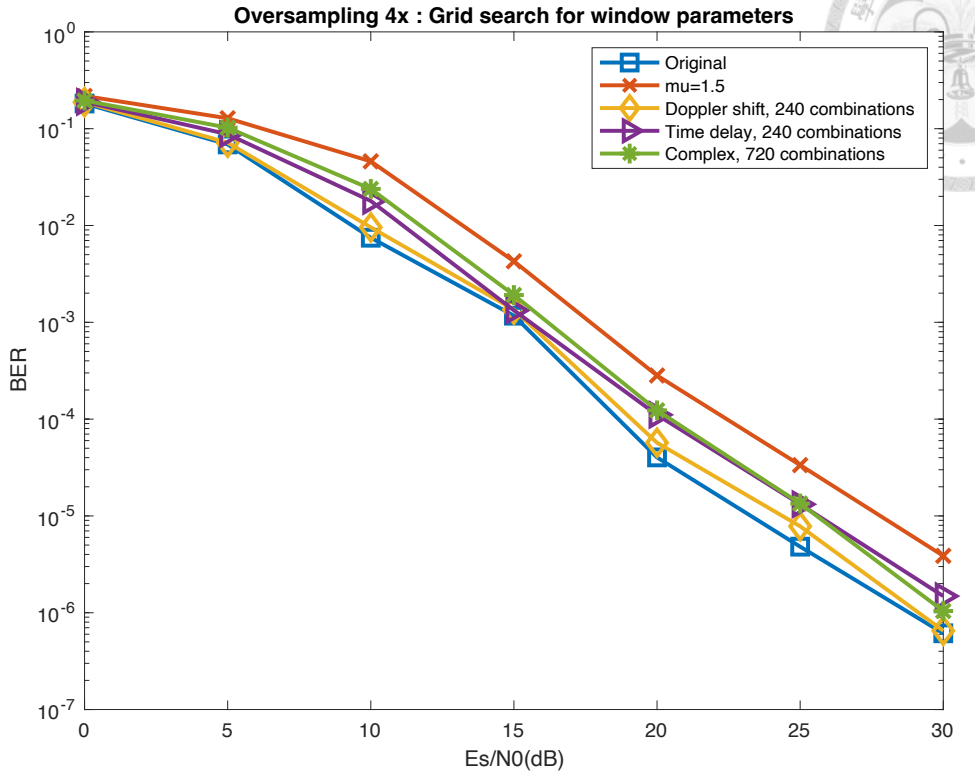

Figure 4.11 The BER curves of different windows whose parameters chosen by grid search (with oversampling)

doi:10.6342/NTU202402900

Chapter 5 Conclusion and future work

5.1 Conclusion

In Orthogonal Time Frequency Space (OTFS) systems, reducing Peak-to-Average Power Ratio (PAPR) is critical for improving signal quality and power efficiency.[1] High PAPR can lead to non-linear distortions in power amplifiers, which degrade system performance. Conventional techniques like the μ-law companding method, while effective in PAPR reduction, often introduce significant Bit Error Rate (BER) degradation.

To address these challenges, our study explored the use of three types of windowing techniques: Doppler shift window, time delay window, and complex window. Each window type was evaluated using different parameter selection methods, including grid search and derived parameters. Our experiments demonstrated the effectiveness and advantages of these window techniques in reducing PAPR. The complex window, in particular, showed the highest PAPR reduction while maintaining a BER advantage over the μ-law method. This validates our hypothesis that windowing can be effectively integrated into OTFS systems to enhance their performance without the substantial BER penalties typically associated with traditional PAPR reduction methods.

5.2 Future work

doi:10.6342/NTU202402900

Future research directions could focus on the further optimization of window parameters to maximize PAPR reduction while keeping BER at acceptable levels. Advanced optimization algorithms and machine learning techniques could be explored to fine-tune the window parameters more efficiently. Additionally, the minimal impact on BER observed with the window techniques opens up the possibility of combining these methods with other existing PAPR reduction techniques. By integrating windowing methods with techniques such as tone reservation, active constellation extension, or selective mapping, we could potentially achieve even greater improvements in PAPR reduction and overall system performance.

doi:10.6342/NTU202402900

Reference

[1] S. R. R. Hadani, S. Kons, M. Tsatsanis,, C. I. A. Monk, J. Delfeld, Y. Hebron,, and A. F. M. A. J. Goldsmith, and R. Calderbank, "Orthogonal Time Frequency Space Modulation," 2018.

[2] S. K. a. S. Deshwala, "A Review on Orthogonal Time Frequency Space Modulation," 2021.

[3] V. S. Cheemala Naveen, "Peak-to-Average Power Ratio reduction in OTFS modulation using companding technique," 2020.

[4] G. D. Surabhi, R. M. Augustine, and A. Chockalingam, "Peak-to-Average Power Ratio of OTFS Modulation," *IEEE Communications Letters,* vol. 23, no. 6, pp. 999-1002, 2019, doi: 10.1109/lcomm.2019.2914042.

[5] H. Bitra, P. Ponnusamy, S. Chintagunta, and S. Pragadeshwaran, "Nonlinear companding transforms for reducing the PAPR of OTFS signal," *Physical Communication,* vol. 53, 2022, doi: 10.1016/j.phycom.2022.101729.

[6] S. Li, W. Yuan, Z. Wei, R. Schober, and G. Caire, "Orthogonal Time Frequency Space Modulation—Part II: Transceiver Designs," *IEEE Communications Letters,* vol. 27, no. 1, pp. 9-13, 2023, doi: 10.1109/lcomm.2022.3209683.

[7] P. Du and Y. Zhang, "Joint precoding and equalization design for reduced-CP OTFS based on the compact input–output model," *Physical Communication,* vol. 53, 2022, doi: 10.1016/j.phycom.2022.101748.

[8] S. E. Zegrar and H. Arslan, "A Novel Cyclic Prefix Configuration for Enhanced Reliability and Spectral Efficiency in OTFS Systems," *IEEE Wireless Communications Letters,* vol. 12, no. 5, pp. 888-892, 2023, doi: 10.1109/lwc.2023.3247893.

[9] P. Raviteja, Y. Hong, E. Viterbo, and E. Biglieri, "Practical Pulse-Shaping Waveforms for Reduced-Cyclic-Prefix OTFS," *IEEE Transactions on Vehicular Technology,* vol. 68, no. 1, pp. 957-961, 2019, doi: 10.1109/tvt.2018.2878891.

[10] P. Raviteja, K. T. Phan, Y. Hong, and E. Viterbo, "Interference Cancellation and Iterative Detection for Orthogonal Time Frequency Space Modulation," *IEEE Transactions on Wireless Communications,* vol. 17, no. 10, pp. 6501-6515, 2018, doi: 10.1109/twc.2018.2860011.

[11] A. Farhang, A. RezazadehReyhani, L. E. Doyle, and B. Farhang-Boroujeny, "Low Complexity Modem Structure for OFDM-Based Orthogonal Time Frequency Space Modulation," *IEEE Wireless Communications Letters,* vol. 7, no. 3, pp. 344-347, 2018, doi: 10.1109/lwc.2017.2776942.

doi:10.6342/NTU202402900

[12] Y. L. Lingjun Li, Pingzhi Fan,Yongliang Guan, "Low Complexity Detection Algorithms for OTFS under Rapidly Time-varying Channel," 2019.

[13] K. R. M. a. A. Chockalingam, "On OTFS Modulation for High-Doppler Fading Channels," 2018.

[14] G. D. Surabhi and A. Chockalingam, "Low-Complexity Linear Equalization for OTFS Modulation," *IEEE Communications Letters,* vol. 24, no. 2, pp. 330-334, 2020, doi: 10.1109/lcomm.2019.2956709.

[15] S. Tiwari, S. S. Das, and V. Rangamgari, "Low complexity LMMSE Receiver for OTFS," *IEEE Communications Letters,* vol. 23, no. 12, pp. 2205-2209, 2019, doi: 10.1109/lcomm.2019.2945564.

[16] S. T. Vivek Rangamgari*, Suvra Sekhar Das*, and Subhas Chandra Mondal†, "OTFS_Interleaved OFDM with Block CP," 2020.

[17] Ying-Che Hung and Shang-Ho (Lawrence) Tsai, "PAPR Analysis and Mitigation Algorithms for Beamforming MIMO OFDM Systems," *IEEE Transactions on Wireless Communications,* vol. 13, no. 5, pp. 2588-2600, 2014, doi: 10.1109/twc.2014.031914.130347.

[18] P. Wei, Y. Xiao, W. Feng, N. Ge, and M. Xiao, "Charactering the Peak-to-Average Power Ratio of OTFS Signals: A Large System Analysis," *IEEE Transactions on Wireless Communications,* vol. 21, no. 6, pp. 3705-3720, 2022, doi: 10.1109/twc.2021.3123397.

[19] A. Kumar, N. Gaur, S. Chakravarty, and A. Nanthaamornphong, "Reducing the PAPR of OTFS Modulation Using Hybrid PAPR Algorithms," *Wireless Personal Communications,* vol. 133, no. 4, pp. 2503-2523, 2024, doi: 10.1007/s11277-024-10885-y.

[20] M. N. Hossain, Y. Sugiura, T. Shimamura, and H.-G. Ryu, "DFT-Spread OTFS Communication System with the Reductions of PAPR and Nonlinear Degradation," *Wireless Personal Communications,* vol. 115, no. 3, pp. 2211-2228, 2020, doi: 10.1007/s11277-020-07678-4.

[21] S. Gao and J. Zheng, "Peak-to-Average Power Ratio Reduction in Pilot-Embedded OTFS Modulation Through Iterative Clipping and Filtering," *IEEE Communications Letters,* vol. 24, no. 9, pp. 2055-2059, 2020, doi: 10.1109/lcomm.2020.2993036.

doi:10.6342/NTU202402900